Title

Visual stimulation induces distinct forms of sensitization of On-Off direction-selective ganglion cell responses in the dorsal and ventral retina.

Journal

Journal of Neuroscience, 42(22)

ISSN

0270-6474

Authors

Huang □□□, Xiaolin
Kim, Alan Jaehyun
Acarón Ledesma, Héctor
et al.

Publication Date

2022-06-01

DOI

10.1523/jneurosci.1391-21.2022

Peer reviewed

Systems/Circuits

Visual Stimulation Induces Distinct Forms of Sensitization of On-Off Direction-Selective Ganglion Cell Responses in the Dorsal and Ventral Retina

Xiaolin Huang (黄晓霖),[1,2] Alan Jaehyun Kim,[1] Héctor Acarón Ledesma,[1,3] Jennifer Ding,[1,2] Robert G. Smith,[4] and Wei Wei[1]

[1]Department of Neurobiology, The University of Chicago, Chicago, Illinois 60637, [2]The Committee on Neurobiology Graduate Program, The University of Chicago, Chicago, Illinois 60637, [3]Graduate Program in Biophysical Sciences, University of Chicago, Chicago, Illinois 60637, and [4]Department of Neuroscience, Perelman School of Medicine, University of Pennsylvania, Philadelphia, Pennsylvania 19104

Experience-dependent modulation of neuronal responses is a key attribute in sensory processing. In the mammalian retina, the On-Off direction-selective ganglion cell (DSGC) is well known for its robust direction selectivity. However, how the On-Off DSGC light responsiveness dynamically adjusts to the changing visual environment is underexplored. Here, we report that On-Off DSGCs tuned to posterior motion direction [i.e. posterior DSGCs (pDSGCs)] in mice of both sexes can be transiently sensitized by prior stimuli. Notably, distinct sensitization patterns are found in dorsal and ventral pDSGCs. Although responses of both dorsal and ventral pDSGCs to dark stimuli (Off responses) are sensitized, only dorsal cells show the sensitization of responses to bright stimuli (On responses). Visual stimulation to the dorsal retina potentiates a sustained excitatory input from Off bipolar cells, leading to tonic depolarization of pDSGCs. Such tonic depolarization propagates from the Off to the On dendritic arbor of the pDSGC to sensitize its On response. We also identified a previously overlooked feature of DSGC dendritic architecture that can support dendritic integration between On and Off dendritic layers bypassing the soma. By contrast, ventral pDSGCs lack a sensitized tonic depolarization and thus do not exhibit sensitization of their On responses. Our results highlight a topographic difference in Off bipolar cell inputs underlying divergent sensitization patterns of dorsal and ventral pDSGCs. Moreover, substantial crossovers between dendritic layers of On-Off DSGCs suggest an interactive dendritic algorithm for processing On and Off signals before they reach the soma.

Key words: **direction-selective ganglion cell; direction selectivity; retina; retinal circuitry; sensitization and adaptation; visual processing**

Significance Statement

Visual neuronal responses are dynamically influenced by the prior visual experience. This form of plasticity reflects the efficient coding of the naturalistic environment by the visual system. We found that a class of retinal output neurons, On-Off direction-selective ganglion cells, transiently increase their responsiveness after visual stimulation. Cells located in dorsal and ventral retinas exhibit distinct sensitization patterns because of different adaptive properties of Off bipolar cell signaling. A previously overlooked dendritic morphologic feature of the On-Off direction-selective ganglion cell is implicated in the cross talk between On and Off pathways during sensitization. Together, these findings uncover a topographic difference in the adaptive encoding of upper and lower visual fields and the underlying neural mechanism in the dorsal and ventral retinas.

Received July 6, 2021; revised Apr. 15, 2022; accepted Apr. 19, 2022.

Author contributions: X.H. and W.W. designed research; X.H., A.J.K., H.A.L., J.D., and R.G.S. performed research; H.A.L. and R.G.S. contributed unpublished reagents/analytic tools; X.H., A.J.K., and R.G.S. analyzed data; X.H. and W.W. wrote the paper.

This work was supported by National Institutes of Health (NIH) Grants R01-EY-02416 and R01-NS-109990, and the McKnight Scholarship Award to W.W.; National Science Foundation Graduate Research Fellowship Program Grant DGE-1746045 to J.D.; NIH Grant F31-EY029156 to H.A.L.; and NIH EY022070 to R.G.S. We thank Chen Zhang for managing the mouse colony.

X. Huang's present address: Division of Neurobiology, Department of Molecular and Cell Biology, Helen Wills Neuroscience Institute, University of California, Berkeley, CA 94720.

H. Acarón Ledesma's present address: F.M. Kirby Neurobiology Center, Boston Children's Hospital, Harvard Medical School, Boston, MA 02115.

J. Ding's present address: Department of Neurobiology, Harvard Medical School, Boston, MA 02115.

The authors declare no competing financial interests.

Correspondence should be addressed to Wei Wei at weiw@uchicago.edu.

https://doi.org/10.1523/JNEUROSCI.1391-21.2022

Introduction

Visual perception and visual neuronal responses are dynamically influenced by prior visual stimuli. Such short-term modulation is thought to underlie some visual perceptual phenomena such as saliency-based bottom-up visual attention and a rich repertoire of aftereffects and illusions (Clifford et al., 2000; Kohn, 2007; Schwartz et al., 2007; Theeuwes, 2013; Barchini et al., 2018; Kamkar et al., 2018; Akyuz et al., 2020). In the early stage of the vertebrate visual system, retinal ganglion cells (RGCs) already show short-term adjustments of their responsiveness. Previous studies have mainly focused on adaptation, which refers to the decrease of sensitivity after a period of strong stimulus (Kim and Rieke, 2001; Demb, 2008; Rieke and Rudd, 2009; Wark et al., 2009; Khani and Gollisch, 2017; Matulis et al., 2020). However, sensitization, the enhanced responsiveness after a strong stimulus, has been documented more recently. Studies in zebrafish, salamander, mouse, and primate show that subpopulations of RGCs transiently increase their sensitivity after a period of high-contrast stimulation (Kastner and Baccus, 2011; Nikolaev et al., 2013; Appleby and Manookin, 2019). The phenomenon of RGC sensitization is conserved across species, suggesting its functional significance. Sensitization has been proposed to complement adaptation for maintaining the responsiveness of the overall RGC population and improving the information-encoding capacity and fidelity, and to contribute to the prediction of future visual inputs (Kastner and Baccus, 2011, 2013; Appleby and Manookin, 2019; Kastner et al., 2019).

The RGC population consists of diverse cell types, each conveying a distinct feature to the brain (Sanes and Masland, 2015). Delineating the sensitization or adaptation patterns of specific RGC types is thus necessary for a more comprehensive understanding of the neural code of the retina. In the mammalian retina, On-Off direction-selective ganglion cells (DSGCs) are well defined encoders of the direction of motion, exhibiting a strong response to motion in their preferred direction but a weak response to motion in the opposite direction (null direction; Barlow and Levick, 1965). They project to both the dorsal lateral geniculate nucleus in the visual thalamus and the superior colliculus (Huberman et al., 2009; Kay et al., 2011; Rivlin-Etzion et al., 2011; Cruz-Martín et al., 2014), and contribute to visual processing in these target areas (Litvina and Chen, 2017; Shi et al., 2017; Liang et al., 2018). However, how the light sensitivity of these cells is shaped by prior visual stimuli is not fully understood.

The On and Off responses of On-Off DSGCs are generated in different layers of their bistratified dendritic arbors, which are embedded in the On and Off sublaminae of the inner plexiform layer (IPL). The synaptic inputs onto each dendritic layer consist of glutamatergic inputs from On or Off bipolar cells, cholinergic inputs, and asymmetric GABAergic inputs from On or Off starburst amacrine cells (SACs). The GABAergic inhibition is strongest when motion is in the null direction, but weakest and delayed in the preferred direction, and thus plays an essential role in the direction tuning of DSGCs (Barlow and Levick, 1965). Although mechanisms underlying direction selectivity have been extensively studied, the adaptation or sensitization properties of the synaptic inputs of DSGC, and the resulting impacts on its spiking activity are not well understood. Notably, previous studies show that a brief period of visual stimulation can lead to a stable change in DSGC directional tuning, with a subset of cells reversing their preferred directions (Rivlin-Etzion et al., 2012). However, reversible adaptive properties of DSGCs have not been thoroughly examined.

In this study, we address these outstanding questions by monitoring the synaptic inputs and spiking activity of posterior DSGCs (pDSGCs) before and after a period of visual stimulation. We found that a set of isocontrast stimuli can induce the sensitization of synaptic inputs onto DSGCs and cause enhanced spiking responses without changes in directional tuning. Surprisingly, we found that dorsal and ventral pDSGCs exhibit distinct sensitization patterns that originate from the Off pathway. In contrast to the conventional view of segregated signal processing in the On and Off dendritic layers of the DSGC, we noted substantial dendritic crossovers between layers that may contribute to the relay of sensitization from the Off to the On pathway in the dorsal pDSGC. Together, these results reveal location-dependent synaptic mechanisms underlying the divergent sensitization patterns of pDSGCs in the dorsal and ventral retinas.

Materials and Methods

Animals. *Drd4-GFP* mice of ages postnatal day 12 (P12) to P13 or P22 to P53 of both sexes were used in this study to label On-Off DSGCs that prefer motion in the posterior direction (i.e., pDSGCs). This mouse line was originally developed by MMRRC (Mutant Mouse Resource & Research Centers; http://www.mmrrc.org/strains/231/0231.html) on the Swiss Webster background and subsequently was backcrossed to C57BL/6 background. All procedures for mouse maintenance and use were in accordance with the University of Chicago Institutional Animal Care and Use Committee (Protocol no. ACUP 72 247) and in conformance with the National Institutes of Health *Guide for the Care and Use of Laboratory Animals* and the Public Health Service Policy.

Whole-mount retina preparation. Mice were dark adapted for >30 min, anesthetized with isoflurane and then killed by decapitation. Under infrared light, retinas were isolated from the pigment epithelium layers and cut into halves at room temperature in Ames' medium (bubbled with 95% O_2/5% CO_2; Sigma-Aldrich). The retinas were then mounted with ganglion cell layer up on top of a ~1.5 mm^2 hole in a small piece of filter paper (Millipore). Cells in the center of the hole were used for experiments. Throughout the experiment, tissues were kept in the darkness except during visual stimulation, and brief two-photon imaging to find the GFP-expressing cells (<10 s scanning time for each cell).

Visual stimulation. A white organic light-emitting display (OLED; 800 × 600 pixel resolution, delivered to the retina with a scale factor of 1.1 μm/pixel, 60 Hz refresh rate, 470–620 nm; OLEDXL, eMagin) was controlled by an Intel Core Duo computer with a Windows 7 operating system and presented to the retina at a resolution of 1.1 μm/pixel. The OLED visual stimuli were generated using MATLAB and Psychophysics Toolbox (Brainard, 1997). The light spectrum of the OLED did not cover the absorption spectrum of S opsin and thus only activated rhodopsin and M opsins (Wang et al., 2011; Rosa et al., 2016; Warwick et al., 2018). In a subset of the experiments, we replaced the OLED with a UV LED [wavelength (in nanometers): minimum, 397; peak, 405; maximum, 413; FWHM, 12.5; model M405L4, Thorlabs] for S-opsin activation. For stimulation with the UV LED, size of visual stimulus was controlled by a diaphragm with adjustable aperture size placed at the focal plane in the light path. All visual stimuli were projected through the condenser lens of the two-photon microscope focused on the photoreceptor layer and centered on the neuron somas.

The light response of pDSGCs was measured during multiple trials of stationary flashing spots ("the test spot"). For each trial, a white spot 220 μm in diameter was shown for 1 s, followed by 2.5 s of darkness. To measure the baseline light responsiveness, five trials of test spots were presented. And then five trials of one of the following induction stimuli were presented: (1) moving spots (same size and intensity as the test spot; moving area, 660 μm in diameter; speed, 300 μm/s; motion duration, 3 s; inter-motion interval, 2.5 s); (2) 100% contrast square-wave drifting gratings (covering area, 220 μm in diameter; spatial

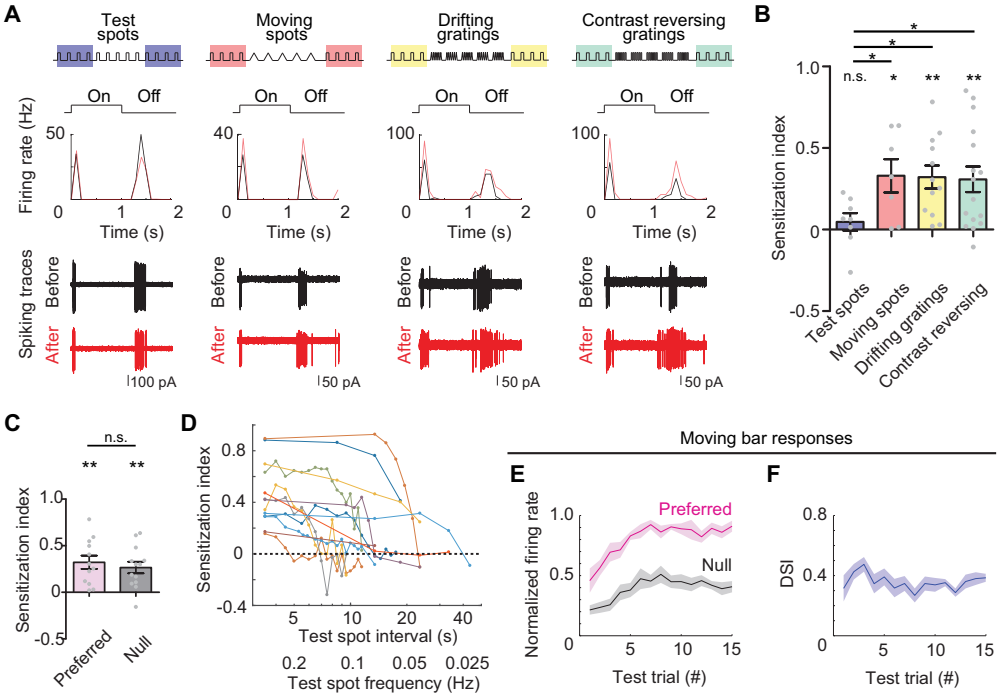

Figure 1. pDSGC responses are transiently sensitized after visual stimulation. ***A***, Example pDSGC responses to 1-s-duration flashing spot stimuli (test spot) before and after five repetitions of test spots, moving spots, and drifting or contrast-reversing gratings stimuli. Top, Schematics of the stimulus protocols. Middle, Firing rates of the example cells before (black) and after (red) different stimulations. Bottom, Overlay of four repetitions of pDSGC spiking traces responding to test spots before and after different stimulations. The test spot has onset at $t = 0$ and offset at $t = 1$ s. ***B***, Summary graph comparing sensitization indices of pDSGC responses after exposure to test spots ($n = 8$ cells from four mice), moving spots in preferred direction ($n = 7$ cells from three mice), drifting gratings in the preferred direction ($n = 12$ cells from 6 mice) or contrast-reversing gratings ($n = 16$ cells from six mice). For this and subsequent plots, data with Gaussian distribution were represented as the mean ± SEM, and gray dots represent individual cells. A one-sample Student's *t* test was used to test whether the sensitization index value of pDSGCs was significantly different from 0, while a two-sample *t* test was used for comparison between control (test spots) and induction visual stimulations. All *p* values were adjusted with FDR correction, as follows: test spots, $p = 0.41$; moving spots, $^*p = 0.031$; drifting gratings, $^{**}p = 0.0056$; contrast-reversing gratings, $^{**}p = 0.0046$; test spots versus moving spots, $^*p = 0.035$; test spots versus drifting gratings, $^*p = 0.027$; test spots versus contrast-reversing gratings, $^*p = 0.044$. ***C***, Comparison of pDSGC sensitization indices after five repetitions of drifting gratings in preferred ($n = 12$ cells from six mice) or null direction ($n = 13$ cells from four mice). Preferred direction, $^{**}p = 0.0024$; null direction, $^{**}p = 0.0017$; preferred versus null, $p = 0.55$. ***D***, Plot of sensitization indices of individual cells with an increasing interval between test spots after the induction stimulus (see also Materials and Methods; $n = 13$ cells from five mice). Individual cells are represented in different colors. ***E***, Normalized firing rate of pDSGCs in preferred and null directions relative to the maximal response of the cell in all trials. Mixed-effects analysis for repeated measurements ($n = 6$ cells from three mice): for preferred response, $^*p = 0.014$; for null response, $^*p = 0.035$. ***F***, DSI of pDSGCs monitored over test trials. Mixed-effects analysis for repeated measurements ($n = 6$ cells from three mice), $p = 0.15$.

frequency, 0.1 cycle/°; temporal frequencies, 1.5 Hz; motion duration, 4 s; inter-motion interval, 1.5 s); and (3) contrast-reversing gratings (covering area, 220 µm in diameter; spatial frequency, 0.1 cycle/°; temporal frequencies, 1.5 Hz; contrast reversing, 4 s; interstimulus interval, 1.5 s). After that, test spots were presented for another 10–60 trials to measure the DSGC light responsiveness after the induction stimulus. If not specifically noted, a drifting grating stimulus in either the preferred or the null direction of the DSGC was used as the default induction stimulus to trigger sensitization effects in this study, as both directions had the same sensitizing effect on DSGCs. For experiments testing the time course of sensitization (Fig. 1*D*), we first presented five repetitions of the regular 3.5-s-interval test spots after the induction stimulus to confirm the degree of sensitization. Then we gradually increased the time interval between test spots and measured the sensitization indexes accordingly. Direction selectivity was tested using either moving bars or drifting gratings at the end of recording, and only cells with robust direction-selective motion responses [mean firing rate of preferred direction response >10 Hz; direction selectivity index (DSI) >0.2; consistent across three repetitions] were included. The intensity of the background (black) was 335 isomerizations [(R*)/rod/s], while both the spots and the bright bars of the gratings had an intensity of $\sim 2.6 \times 10^5$ isomerizations [(R*)/rod/s] in the photopic range. For a subset of experiments using the 405 nm UV LED, see Figure 3; the intensity and the size of the UV test spot were the same as that of the OLED. The induction stimulus with the UV LED was a spot of 220 µm in diameter flashing at 1.5 Hz, with a 4 s flashing duration and a 1.5 s inter-stimulus interval. For a subset of experiments using the visible OLED, we lowered the brightness of the testing spot; the bright peak value of the drifting square-wave gratings was set to 100 R*/rod/s, and the background was 33 R*/rod/s, both of which values were below the cone threshold. For local sensitization experiments, see Figure 8*G*: the OLED stimulus was the same as described above, but the size of the local test spot or area of induction gratings was 66 µm in diameter, centered at 77 µm away from the soma.

Two-photon guided electrophysiology recording. Retinas were perfused with oxygenated Ames' medium with a bath temperature of 32–34°C. GFP-labeled pDSGCs in *Drd4-GFP* mice were targeted using a two-photon microscope (Scientifica) and a Ti:sapphire laser (Spectra-Physics) tuned to 920 nm. Data were acquired using PCLAMP 10 software, a Digidata 1550A digitizer, and a MultiClamp 700B amplifier (Molecular Devices); low-pass filtered at 4 kHz; and digitized at 10 kHz.

For loose cell-attached recordings, electrodes of 3.5–5 MΩ were filled with Ames' medium. For current-clamp whole-cell recording (I = 0), electrodes were filled with a potassium-based internal solution containing 120 mM $KMeSO_4$, 10 mM KCl, 0.07 mM $CaCl_2 \cdot 2H_2O$, 0.1 mM EGTA, 2 mM ATP (magnesium salt), 0.4 mM GTP (trisodium salt), 10 mM HEPES, and 10 mM phosphocreatine (disodium salt), pH 7.25. For voltage-clamp whole-cell recording, electrodes were filled with a cesium-based internal solution containing 110 mM $CsMeSO_4$, 2.8 mM NaCl, 5 mM TEA-Cl, 4 mM EGTA, 4 mM ATP (magnesium salt), 0.3 mM GTP (trisodium salt), 20 mM HEPES, 10 mM phosphocreatine (disodium salt), and 5 mM lidocaine *N*-ethyl chloride (QX314; Sigma-Aldrich), pH 7.25. Light-evoked excitatory postsynaptic currents (EPSCs) and inhibitory postsynaptic currents (IPSCs) of pDSGCs were isolated by holding the

cells at reversal potentials (0 mV for IPSCs and −60 mV for EPSCs). A liquid junction potential (~10 mV) was corrected. To mimic the pDSGC activation pattern during the drifting grating stimulus (see Fig. 5), we selected representative current-clamp recordings of pDSGC membrane potential waveforms during drifting gratings and used them as command potential waveforms in voltage-clamp experiments to replace the visual induction stimulus.

To investigate the contributions of different types of synaptic transmission to pDSGC sensitization, a synaptic agonist or antagonist was included in the Ames' medium: 0.008 mM dihydro-b-erythroidine hydrobromide (DHbE; Tocris Bioscience) for blocking nicotinic cholinergic receptors; 0.002 mM Atropine (Sigma) for blocking muscarinic cholinergic receptors; 0.0125 mM GABAzine (catalog #SR-95 531, Tocris Bioscience) for blocking $GABA_A$ receptors; 0.001 mM strychnine (Sigma-Aldrich) for blocking glycinergic receptors; and 0.005 mM L-AP-4 (Tocris Bioscience) for activating type 6 metabotropic glutamatergic receptors (mGluR6s) and blocking the On signaling pathways.

Analysis of electrophysiological data. For the measurement of the baseline light responsiveness, five repetitions of test spots were presented. Responses during the second to the fifth test spots were averaged as baseline light responses (N_{Before}), and the response during the first test spot was discarded to avoid the impact of fast adaptation after onset of the visual stimulus from long-term dark adaptation (Baccus and Meister, 2002). Sensitization index $= \frac{N_{After} - N_{Before}}{N_{After} + N_{Before}}$ was used to quantify the strength of sensitization, where N is the averaged pDSGC response to the four test spots right before (N_{Before}) and after (N_{After}) the period of stationary flash spots (same as test spots), moving spots, drifting gratings, or contrast-reversing grating stimuli. A higher positive sensitization index value indicates stronger sensitization, while a negative sensitization index value indicates adaptation. N is the firing rate for loose cell-attached recording data, the subthreshold integral area for postsynaptic potentials (PSPs), and peak amplitude for PSCs.

The time windows used to separate On, Off, and sustained components were determined by the EPSC waveforms of dorsal pDSGCs, which had three clear peaks. The mean of the boundary between the Off and the sustained components was ~700 ms ($n = 8$ cells from six mice). Defining the onset of the test spot as $t = 0$, the On response time window was 0–1 s; the Off response time window was 1–1.7 s; and the sustained component time window was 1.7–3 s. The same time windows were used for analyzing spiking, PSP, and PSC data of both dorsal and ventral pDSGCs. Current and voltage responses were continuously recorded with two 30 s baseline windows before and after the sensitization protocol. The baseline of the whole trace was averaged from the two baseline windows recorded during the no-stimulus period.

Data were analyzed using PCLAMP 10, MATLAB, and GraphPad Prism. For whole-cell patch-clamp recordings, membrane tests were performed to check the recording quality, and recordings with series resistances >25 MΩ or a ratio of membrane resistance to series resistance <10 were discarded.

Dendritic tracing. GFP-labeled pDSGCs in *Drd4-GFP* mice were targeted using a two-photon microscopy and filled with 25 μM Alexa Fluor 594 (Thermo Fisher Scientific). DSGC dendrites were traced from *z*-stacked images in ImageJ using the open source software Simple Neurite Tracer. On and Off layers were identified and separated using NeuronStudio, and then dendritic length and dendritic arbor diameter (El-Danaf and Huberman, 2019) were calculated in MATLAB.

Two criteria were used to determine a dendritic segment as a crossover dendrite originating from one layer into the other: (1) the dendrite had at least 5 μm of segments remaining in the original layer before diving down; and (2) the dendrite crossed over the gap between two layers and stratified into the other layer. The crossover dendrites were then classified into four subtypes labeled in the following different colors (see Fig. 8): red, Off dendrites originated from On dendrites ("Off from On"); yellow, On dendrites originated from Off dendrites ("On from Off"); blue, On dendrites originated from the red "Off from On" crossover dendrites ["On from Off (from On)"]; and magenta, Off dendrites originated from the yellow "On from Off" crossover dendrites ["Off from On (from Off)"].

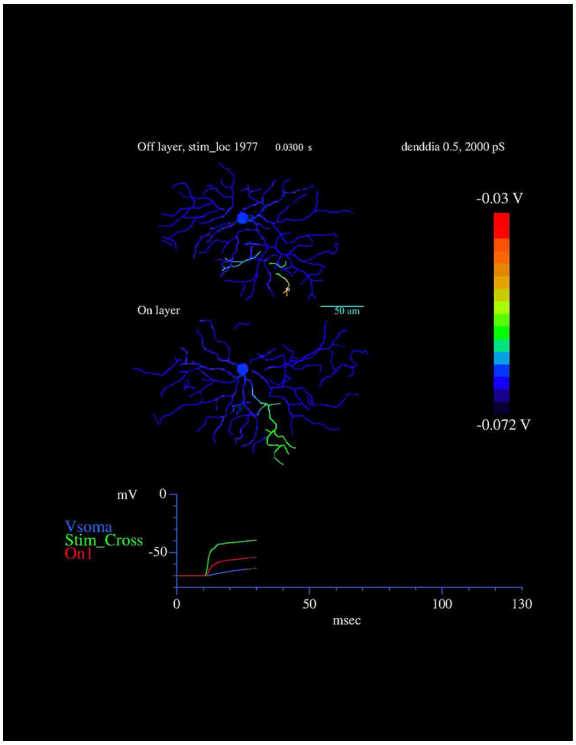

Movie 1. Passive electrotonic spread between pDSGC Off and On layers upon a single synaptic input onto the Off dendrites. The heat map representing the membrane potential of pDSGC after stimulation in the Off layer (I_s: 70 pA, 100 ms). The stimulated location #1977 is indicated by *. Ri = 100 Ωcm; dendritic dia factor = 0.5. [View online]

Computational simulation. Models of the pDSGC were developed from a real ganglion cell morphology (see Fig. 8*B*, the cell) that had been reconstructed from two-photon images. The dendritic diameters were adjusted by multiplying by a constant termed the "dendritic dia factor" (0.3–0.8; typically, 0.5) to correct for the enlargement of dendrite diameter during imaging. The morphology was discretized into a compartmental model (compartment size = 0.01–0.02 λ; ~1100–2200 compartments; Ri = 50–200 Ωcm (typically, 100 Ωcm); Rm = 20,000 Ωcm^2; Vrev = −70 mV). In the passive model, voltage-gated ion channels and NMDA receptors were removed to simulate subthreshold behavior in the pDSGC [Movies 1, 2, 3, 4, 5, 6, 7, 8, 9, 10, 11, 12, 13, 14, 15, 16, 17, 18, 19). In active models, NMDA receptors and a somatic spiking mechanism (Movies 11, 12, 13), or NMDA receptors and a dendritic spiking mechanism (Movies 14, 15, 16) were included. Movies were generated by displaying the morphology as two separate images, each showing one of the pDSGC dendritic arborization layers, and the dendritic membrane voltage was displayed as a heat map. The movie frame interval was 1 ms. The model simulations and movies were constructed with the simulation language Neuron-C (Smith, 1992). In Movies 1, 2, 3, 4, 5, 6, 7, 8, 9, 10 using the passive model, the stimulus was a current clamp (70 pA; duration, 100 ms) that represented a bipolar cell input. These pDSGC models were stimulated at one dendritic location, and simultaneously the evoked membrane voltages were recorded at another set of locations. In Movies 11, 12, 13, 14, 15, 16, 17, 18, 19, an Off spot stimulus (diameter, 100 μm; duration, 50 ms) activated bipolar cell inputs onto regions of the pDSGC dendrites to simulate the sensitized Off response with a sustained component, and then after 20 ms an On spot stimulus (diameter, 100 μm; duration, 10 ms) was delivered to the same site or a distant site. Locations of the spots (*x*, *y*; in micrometers) were as follows: spot 1: 80, 20; spot 2: 20, −60; spot 4: −60, −50. The postsynaptic conductances of the bipolar cell inputs in the pDSGC ranged from 200 to 3500 pS, with a reversal potential of 0 mV.

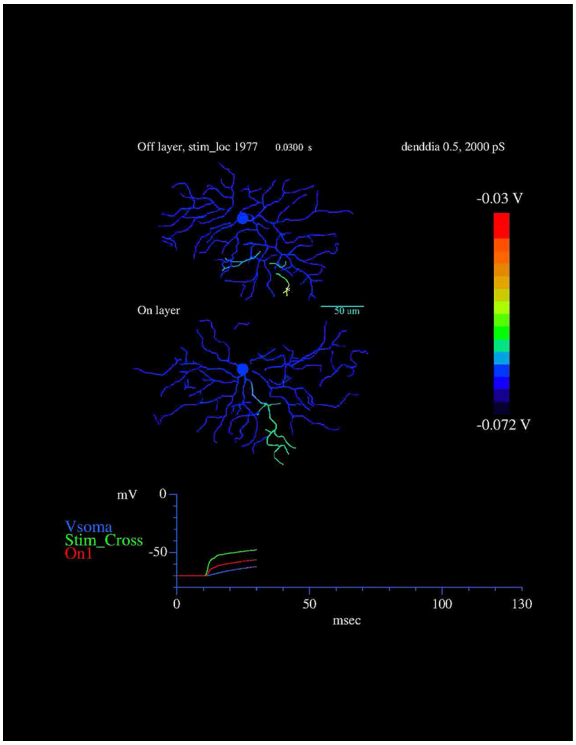

Movie 2. Electrotonic spread of depolarization between pDSGC dendritic layers with smaller Ri. Stimulation with the same I_s, dendritic location, and dendritic dia factor as that in Movie 1, but with smaller Ri (50 Ωcm). [View online]

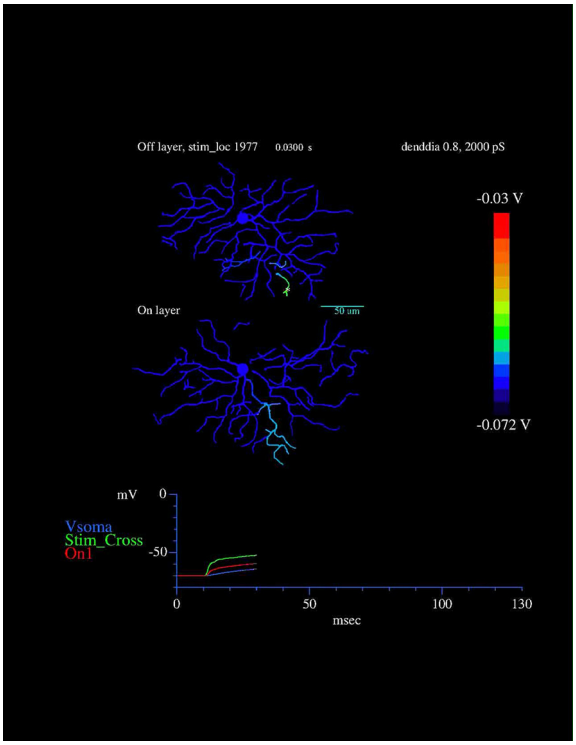

Movie 4. Electrotonic spread of depolarization between pDSGC dendritic layers with smaller dendritic dia factor. Stimulation with the same I_s, dendritic location, and Ri as that in Movie 1, but with smaller dendritic dia factor (0.3). [View online]

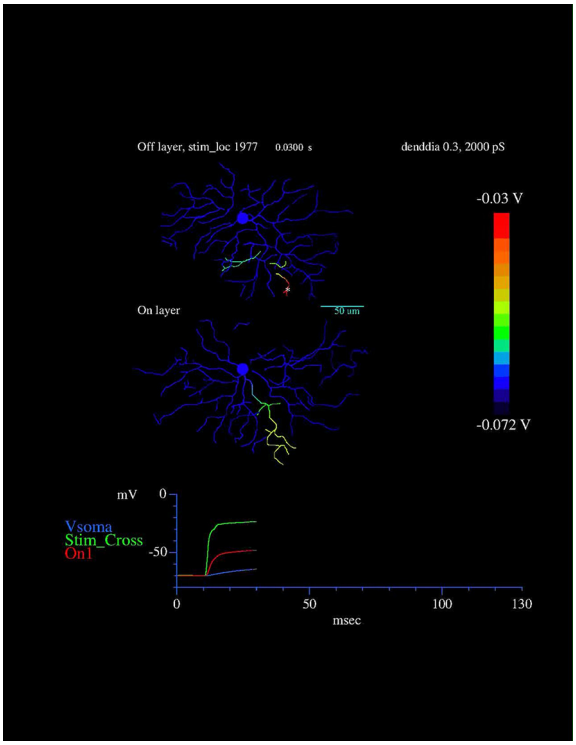

Movie 3. Electrotonic spread of depolarization between pDSGC dendritic layers with bigger Ri. Stimulation with the same I_s, dendritic location, and dendritic dia factor as that in Movie 1, but with bigger Ri (200 Ωcm). [View online]

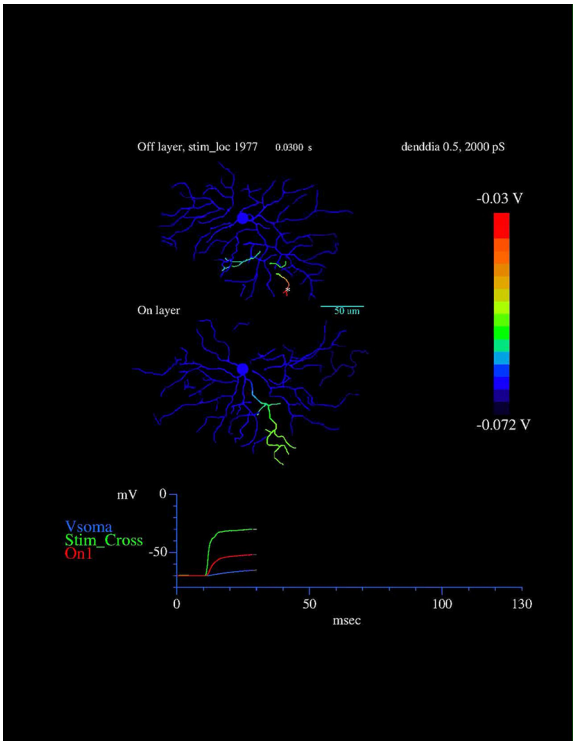

Movie 5. Electrotonic spread of depolarization between pDSGC dendritic layers with bigger dendritic dia factor. Stimulation with the same I_s, dendritic location, and Ri as that in Movie 1, but with bigger dendritic dia factor (0.8). [View online]

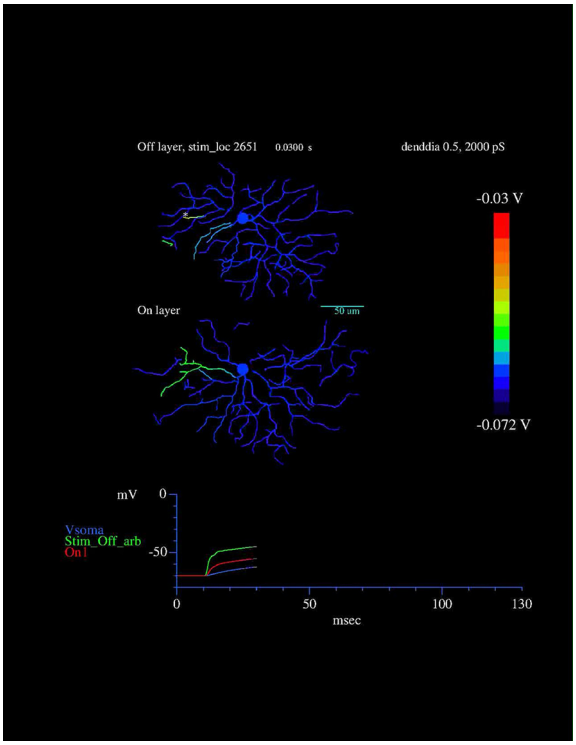

Movie 6. Electrotonic spread of depolarization between pDSGC dendritic layers with a different stimulation location. Color maps of pDSGC membrane potentials after stimulation at location (#328) in the Off layer. The stimulation parameters (I_s, Ri, and dendritic dia factor) are the same as those in Movie 1. [View online]

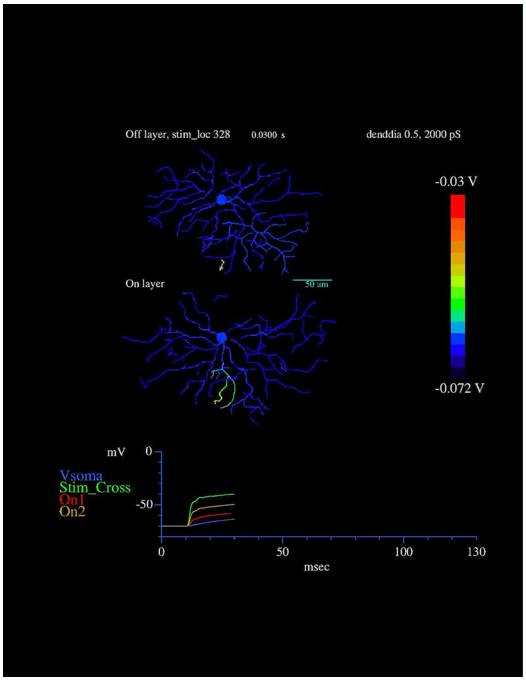

Movie 7. Electrotonic spread of depolarization between pDSGC dendritic layers with a different stimulation location. Stimulation at location (#2450) in the Off layer. The stimulation parameters (I_s, Ri, and dendritic dia factor) are the same as those in Movie 1. [View online]

Experimental design and statistical analysis. The sample size in each group was calculated based on preliminary data to have a power of test stronger than 0.8. Grouped data with Gaussian distribution were presented as the mean ± SEM in summary graphs, with scattered dots

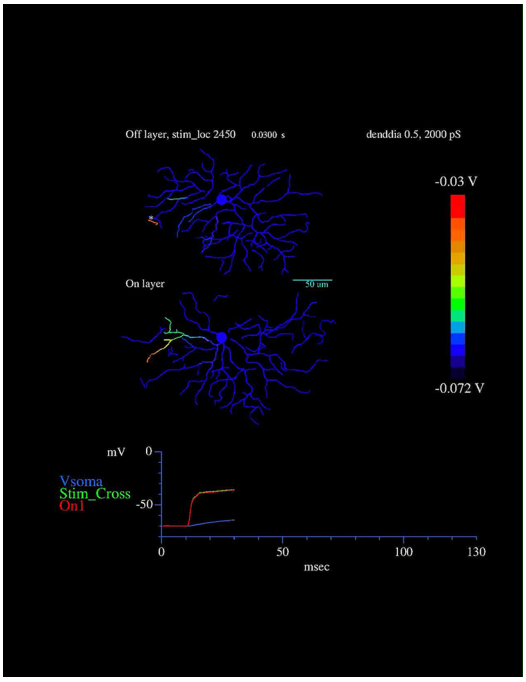

Movie 8. Electrotonic spread of depolarization between pDSGC dendritic layers with a different stimulation location. Stimulation at location (#2651) in the Off layer. The stimulation parameters (I_s, Ri, and dendritic dia factor) are the same as those in Movie 1. [View online]

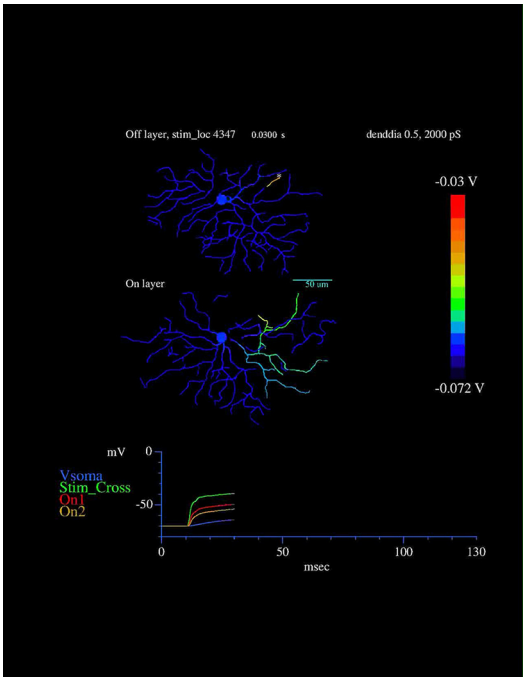

Movie 9. Electrotonic spread of depolarization between pDSGC dendritic layers with a different stimulation location. Stimulation at location (#4347) in the Off layer. The stimulation parameters (I_s, Ri, and dendritic dia factor) are the same as those in Movie 1. [View online]

representing individual cells. A two-sided one-sample t test was performed to test whether the sensitization index value was significantly different from 0, while a two-sided two-sample t test was used to compare two sample groups. Grouped data with non-Gaussian distribution were presented as the median ± interquartile range (IQR) in box plots, and the Kolmogorov–Smirnov test was applied. For multiple comparisons, p values were adjusted with false discovery rate (FDR) correction (Jafari and Ansari-Pour, 2019). A p value <0.05 was considered significant (n.s., no

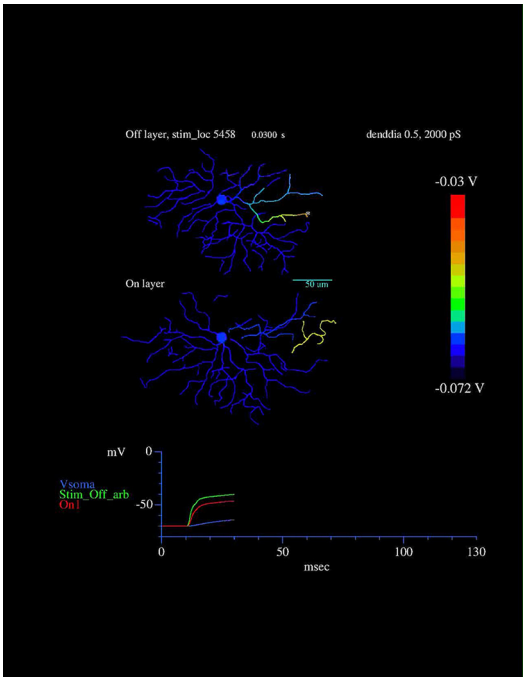

Movie 10. Electrotonic spread of depolarization between pDSGC dendritic layers with a different stimulation location. Stimulation at location (#5458) in the Off layer. The stimulation parameters (I_s, Ri, and dendritic dia factor) are the same as those in Movie 1. [View online]

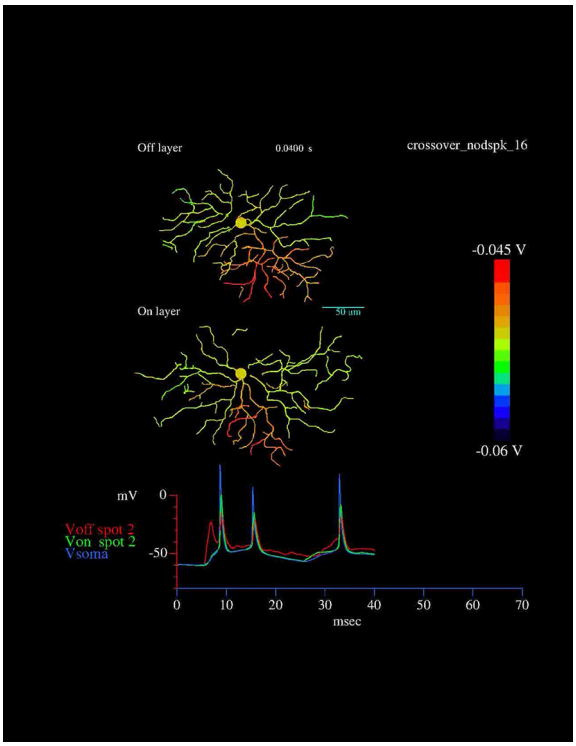

Movie 11. Active pDSGC model with somatic initiation of spiking with Off and On stimuli presented to the same location. Both Off and On spots were presented to location 2. [View online]

significance; $*p < 0.05$; $**p < 0.01$; $***p < 0.001$). The number of experimental repeats were indicated in figure legends.

Data availability. All relevant data collected and analyzed in this study are available from the authors on reasonable request. The NeuronC simulation package and codes for the pDSGC model are available at ftp://retina.anatomy.upenn.edu/pub/nc.tgz.

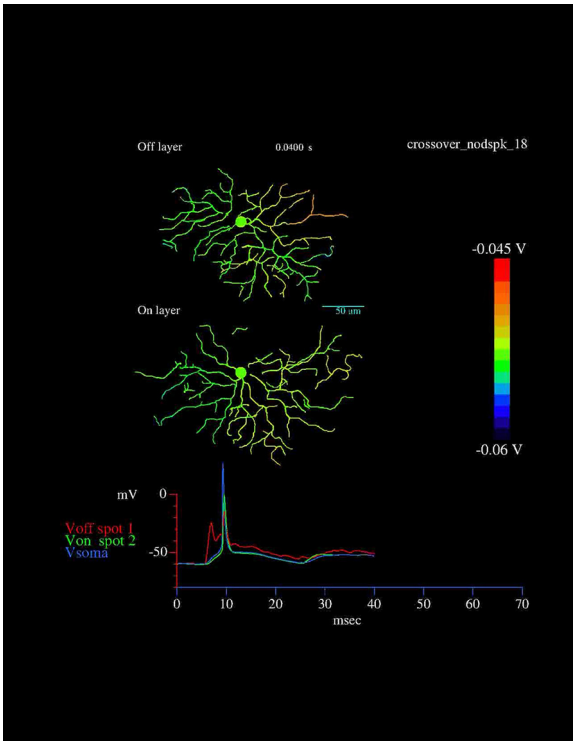

Movie 12. Active pDSGC model with somatic initiation of spiking with Off and On stimuli presented to different locations. Off spots were presented to location 1, while the On dendrite responses were recorded from location 2. [View online]

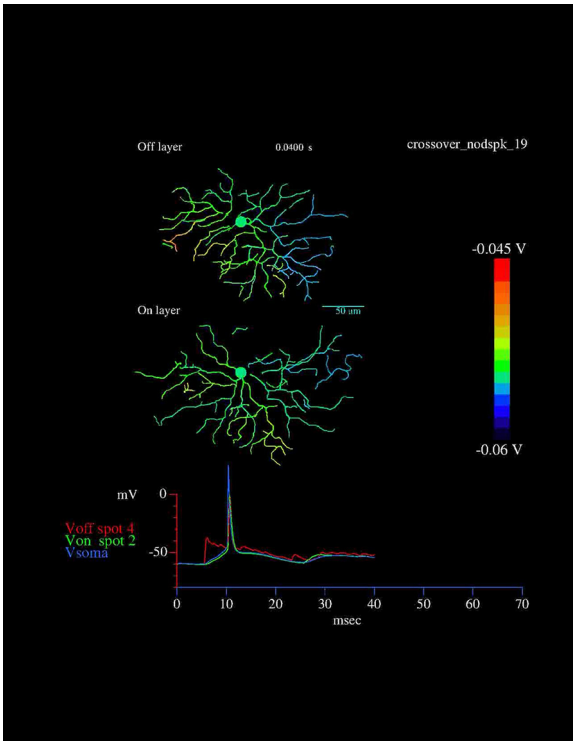

Movie 13. Active pDSGC model with somatic initiation of spiking with Off and On stimuli presented to different locations. Off spots were presented to location 4, while the On dendrite responses were recorded from location 2. [View online]

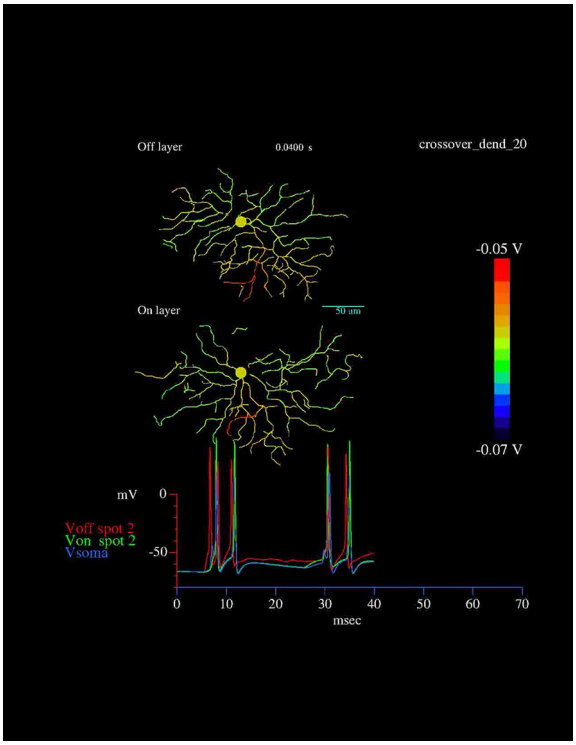

Movie 14. Active pDSGC model with dendritic spiking with Off and On stimuli were presented to the same location. [View online]

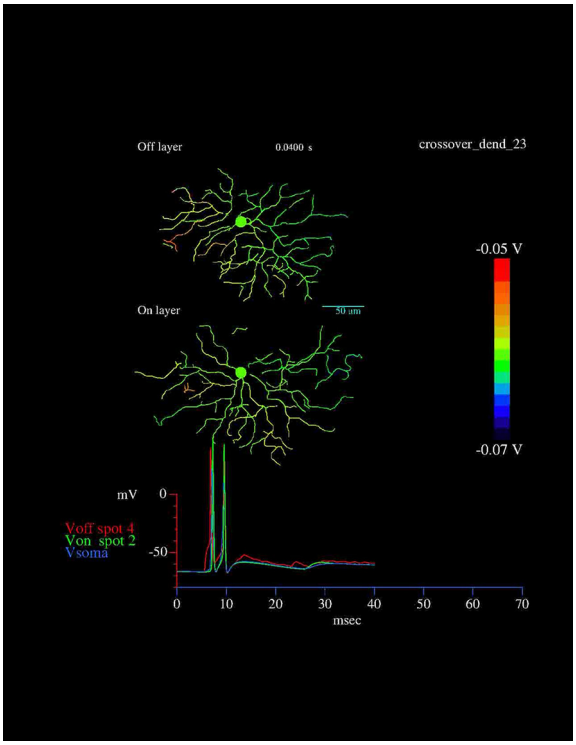

Movie 16. Active pDSGC model with dendritic spiking with Off and On stimuli were presented to different locations. [View online]

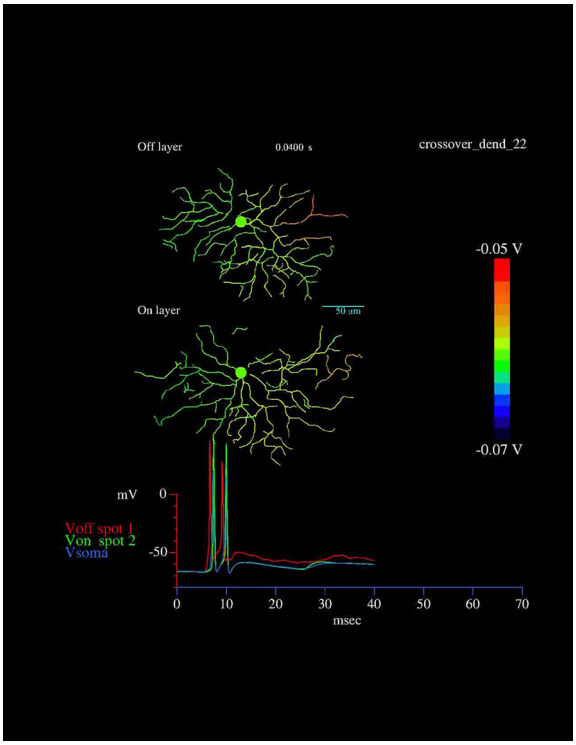

Movie 15. Active pDSGC model with dendritic spiking with Off and On stimuli were presented to different locations. [View online]

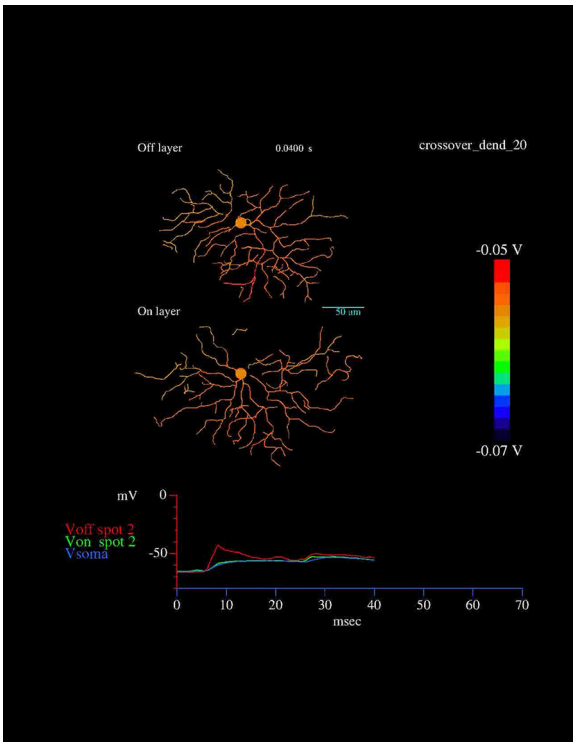

Movie 17. Passive pDSGC model with dendritic spiking with Off and On stimuli were presented to different locations. [View online]

Results

On-Off DSGC light responses can be transiently sensitized after a set of visual stimuli

To examine the influence of prior visual stimuli on the light sensitivity of On-Off DSGCs, we targeted the On-Off DSGC subtype preferring motion in the posterior direction (pDSGCs) in the *Drd4-GFP* transgenic mouse line (Huberman et al., 2009) for patch-clamp recording. We monitored the baseline pDSGC spiking response to a 1 s flashing spot (termed the "test spot")

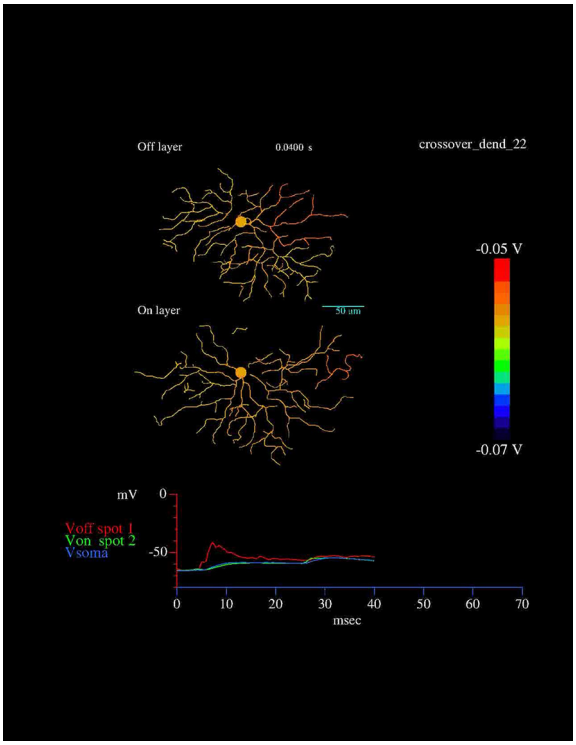

Movie 18. Passive pDSGC model with dendritic spiking when Off and On stimuli were presented 10 different locations. [View online]

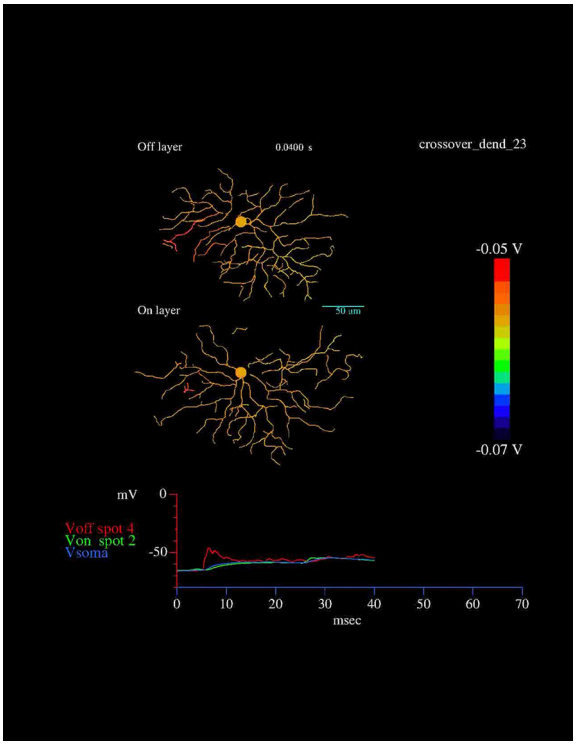

Movie 19. Passive pDSGC model with dendritic spiking when Off and On stimuli were presented to the same location. [View online]

presented every 3.5 s. Then, 27.5 s of visual stimulation (termed the "induction stimulus") was presented to induce sensitization. We tested three types of induction stimuli at the same contrast level as the test spot: preferred direction moving spots, preferred direction drifting gratings, and contrast-reversing gratings (five repetitions of 5.5 s trials, using a white OLED light source; also see Materials and Methods; Fig. 1*A*). Immediately after the induction stimulus, the pDSGC light responsiveness was monitored by trials of the same test spots as those before the induction stimulus. The average firing rates of the pDSGC to the test spot before and after the induction stimulus were then used to calculate a sensitization index, which was defined as (Firing $\text{rate}_{\text{After}}$ − Firing $\text{rate}_{\text{Before}}$)/(Firing $\text{rate}_{\text{After}}$ + Firing $\text{rate}_{\text{Before}}$). Sensitized pDSGC responses are represented as positive sensitization index values, while adapted responses give negative values.

We found that pDSGC spiking responses to test spots were significantly sensitized by all three patterns of induction stimuli. As a control, continuous presentation of test spot trials did not induce sensitization (Fig. 1*A*,*B*). For the rest of this study, we used drifting gratings as the induction stimulus to study the mechanism underlying pDSGC sensitization. Since DSGCs are direction selective, we also tested whether pDSGCs can be sensitized by drifting gratings moving in the null direction. We found that motion in both preferred and null directions can induce similar levels of sensitization in pDSGCs (Fig. 1*C*).

We next investigated the time course of the sensitization and found the following two properties. First, the sensitization is a short-term, reversible phenomenon. We were able to repeatedly induce sensitization in 82% of pDSGCs (14 of 17 cells; Fig. 2, example cell). Second, after the induction stimulus, the sensitization was maintained without decay as long as test spots were presented at an interspot interval of 3.5 s, which was used in our protocol (Fig. 2, the third trial vs the first two trials). In our longest experiment, the pDSGC firing rate to test spots remained sensitized for 210 s. However, in the absence of continuous presentation of test spots, pDSGC light responses decayed back to the baseline level within 5–20 s after the induction of sensitization (Fig. 1*D*; see Materials and Methods).

Moreover, we found that the response of the pDSGC to moving stimuli can also be sensitized. We monitored the spiking activity of pDSGCs during repeated presentation of moving bar trials at the same frequency as the test spots (3.5 s for each trial) in either the preferred or null directions in a pseudorandom manner. We found that pDSGC firing rates in both directions show sensitization during the first six trials of moving bar stimulation before reaching a stable level while the direction selectivity index of the cell remains unchanged (Fig. 1*E*,*F*).

Spiking activities of pDSGCs from the dorsal and the ventral retina show differential patterns of sensitization

Despite an overall increase of spiking activity in all pDSGCs, we noticed that pDSGCs in the dorsal and ventral regions of the retina show distinct sensitization patterns after the induction stimulus (Fig. 3*A*,*B*). We detected sensitized On responses only in the dorsal pDSGCs, but not in the ventral pDSGCs. The Off responses of pDSGCs were sensitized in both the dorsal and ventral groups (Fig. 3*B*,*C*). Notably, in dorsal but not ventral pDSGCs, we also observed elevated baseline spiking activity between trials of test spots, which we termed the "sustained component" (Fig. 3*B*, left, *D*).

A major difference in dorsal and ventral retinas is the ratio of M- and S-opsins coexpressed in cone photoreceptors. M cones in the ventral retina coexpress higher levels of S-opsins compared with dorsal cones (Applebury et al., 2000; Haverkamp et al., 2005; Baden et al., 2013; Rosa et al., 2016), making ventral cones more sensitive to UV light (Wang et al., 2011). However, the white OLED light source we used in this study does not activate

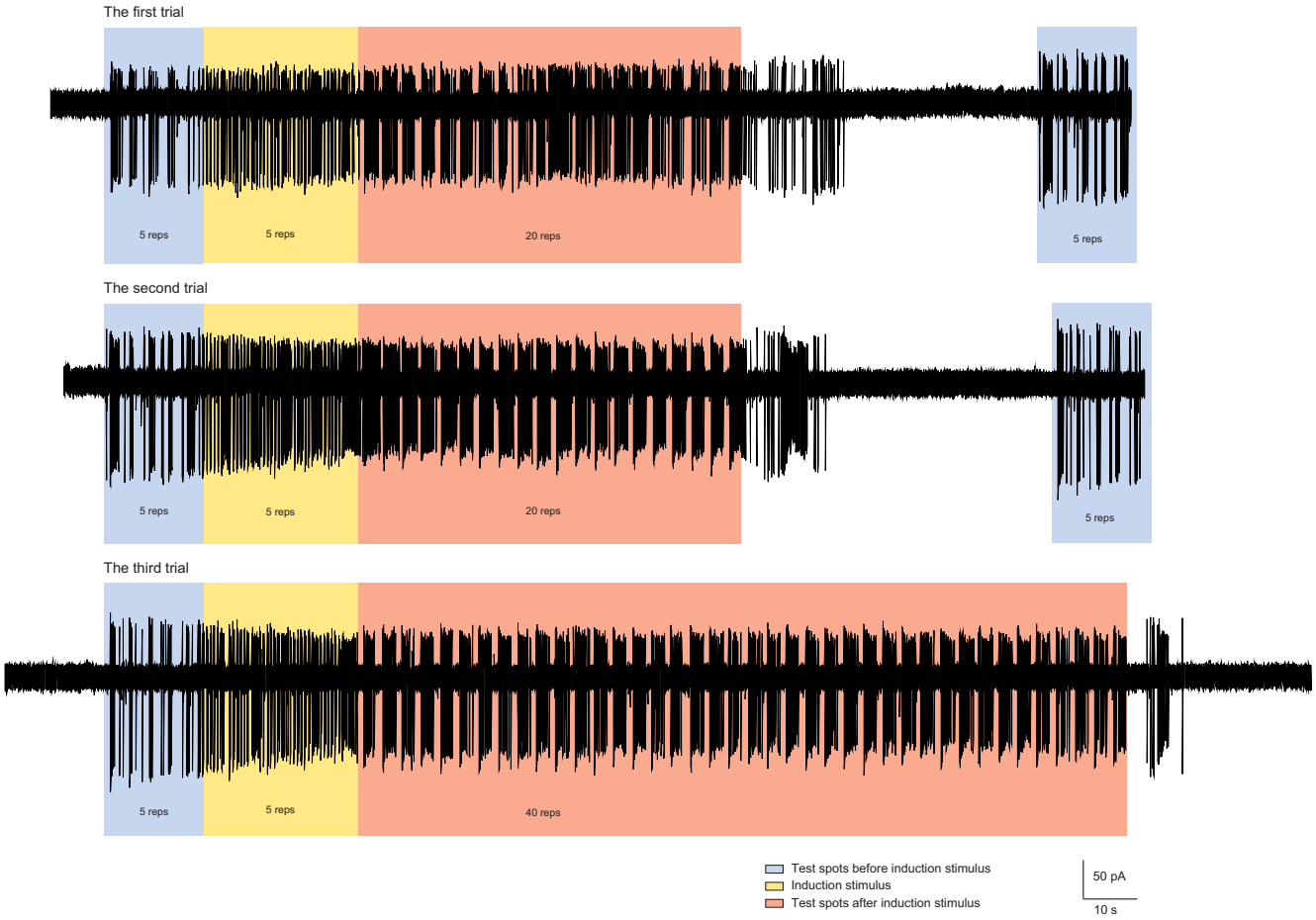

Figure 2. Example spiking traces of a pDSGC represent the maintenance, extinction, and repeated induction of sensitization. Top, middle, and bottom traces represent pDSGC spiking responses during the first, second, and third trial of the induction protocol.

S-opsins (Wang et al., 2011; Rosa et al., 2016). To determine whether the lack of On sensitization and the sustained component in ventral pDSGCs is caused by inadequate cone photoreceptor activation by the OLED in the ventral retina, we replaced the OLED stimulus with a 405 nm UV LED stimulus using the same intensity (see more in Materials and Methods) to activate S-opsins. We observed a UV-induced sensitization pattern of ventral pDSGCs similar to that induced by the OLED: sensitized Off but not On spiking, and a lack of the sustained component (Fig. 3*B*,*C*). UV light did not induce the sustained component in dorsal pDSGCs, presumably because of the lower sensitivity of dorsal photoreceptors to UV light. In another set of experiments, we lowered the maximum intensity of the OLED light source to the rod activation range and recorded from dorsal pDSGCs (see Materials and Methods). Under this condition, there was also no change in pDSGC light response after the induction stimulus (data not shown), indicating that direct activation of cone photoreceptors is necessary for pDSGC sensitization.

In summary, for pDSGCs from the dorsal retina, both On and Off responses were sensitized by the induction stimulus, and there was a sensitized sustained component of spiking between test spot trials. However, for pDSGCs from the ventral retina, there was no sustained component and only Off responses were enhanced after the induction stimulus. This phenomenon was independent of different S-opsin levels in the dorsal and ventral retinas.

Subthreshold membrane potentials of dorsal and ventral DSGCs show distinct sensitization patterns

We next examined membrane depolarization patterns that drive distinct firing patterns of dorsal and ventral pDSGCs using whole-cell current-clamp recording. Spikes were digitally removed to reveal the subthreshold PSPs of pDSGCs (see Materials and Methods). Consistent with the spiking activity, in the dorsal retina, both On and Off PSPs were sensitized after the induction stimulus, while in the ventral retina, only the Off PSPs were sensitized (Fig. 4*B*). Moreover, dorsal pDSGCs exhibited sustained depolarization of their membrane potentials between test spots after the induction stimulus (Fig. 4*A*, *C*), which corresponded to the sensitized sustained component in their spiking activities.

Synaptic inputs of dorsal and ventral DSGCs show differential patterns of sensitization

We hypothesized that the stronger depolarization of the pDSGC membrane potential after the induction stimulus may result from enhanced excitatory inputs or reduced inhibitory inputs. To determine how the synaptic inputs of pDSGCs are modulated by the induction stimulus, we measured the EPSCs and IPSCs of dorsal and ventral pDSGCs using whole-cell voltage-clamp recording. After the induction stimulus, both dorsal and ventral pDSGCs showed enhanced Off EPSC responses (Fig. 4*D*,*E*). The EPSCs of dorsal pDSGCs showed an enhanced On EPSC amplitude (Fig. 4*D*,*E*), as well as an elevated sustained component

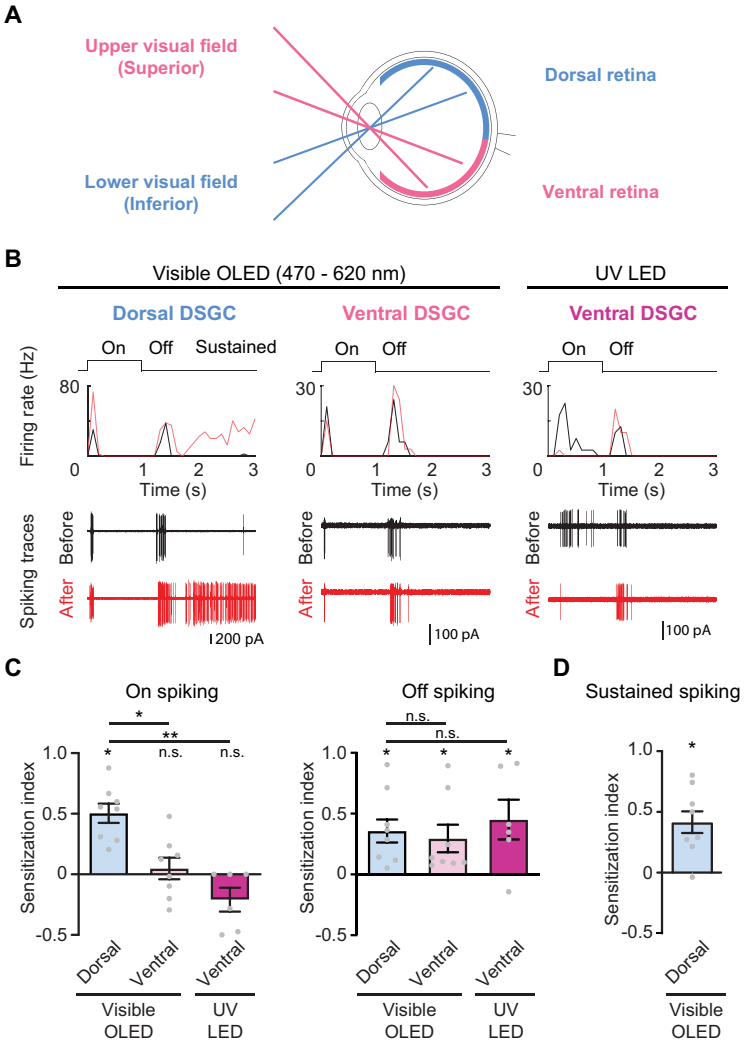

Figure 3. pDSGCs from the dorsal and the ventral retina show differential patterns of sensitization. ***A***, Schematic diagram showing the topographic relationship of dorsal/ventral retinas and the visual fields where they receive visual inputs. ***B***, Firing rate plots and spiking traces of example pDSGCs from the dorsal and the ventral retina responding to test spot stimuli before (black) and after (red) the induction stimulus. ***C***, Summary graphs comparing the sensitization indices of On and Off spiking between pDSGCs from the dorsal and the ventral retina. Dorsal, visible OLED: $n = 8$ cells from three mice; ventral, visible OLED: $n = 8$ cells from four mice; ventral, near-UV LED: $n = 6$ cells from three mice. For On spiking: dorsal, $^{*}p = 0.018$; ventral (visible OLED), $p = 0.70$; ventral (UV), $p = 0.087$; dorsal versus ventral (visible OLED), $^{*}p = 0.037$; dorsal versus ventral (UV), $^{**}p = 0.0016$. For Off spiking: dorsal, $^{*}p = 0.013$; ventral (visible OLED), $^{*}p = 0.049$; ventral (UV), $^{*}p = 0.040$; dorsal versus ventral (visible OLED), $p = 0.68$; dorsal versus ventral (UV), $p = 0.60$. ***D***, Summary graph of sensitization index for the sustained component of dorsal pDSGC spiking activity. $N = 8$ cells from three mice; $^{*}p = 0.011$.

between test spots (Fig. 4*D*,*F*) that corresponded to the sustained component of the spiking activity (Fig. 3*B*,*D*) and of the membrane depolarization (Fig. 4*A*,*C*).

Sensitized spiking activity was not accompanied by reduced inhibition of pDSGCs (Fig. 4*G–I*). In dorsal pDSGCs, we detected an elevated sustained component of the IPSC after the induction stimulus similar to that of the EPSC, suggesting that the sensitization of a sustained excitatory drive to both pDSGCs and a presynaptic inhibitory neuron, likely SACs, which share common bipolar cell inputs (Duan et al., 2014; Kim et al., 2014; Sethuramanujam et al., 2017; Yu et al., 2018).

Taking the above results together, we found that pDSGCs transiently increased their firing after the induction stimulus. The sensitization of the spiking activity is accompanied by enhanced synaptic excitation and membrane depolarization, but not reduced inhibition. Furthermore, in the dorsal retina, sensitized pDSGCs acquired a sustained increase in their synaptic inputs, membrane potential, and spiking activity between test spots.

Synaptic activity is required for the induction of pDSGC sensitization

To investigate the mechanism underlying the induction of pDSGC sensitization, we first tested whether the membrane depolarization of the pDSGC evoked by the induction stimulus was sufficient to trigger sensitization. Instead of using the drifting grating stimulus as the induction stimulus, we mimicked drifting grating-evoked membrane potential changes in dorsal pDSGCs by directly voltage clamping the membrane potential of the pDSGC using the command voltage waveform recorded during the drifting grating stimulus (Fig. 5*A*,*B*). We found that pDSGC EPSCs were not sensitized by this direct depolarization, indicating that sensitization requires visually evoked synaptic inputs (Fig. 5*C*,*D*).

We next investigated which types of synaptic signaling are required for pDSGC sensitization. A major source of synaptic inputs to pDSGCs is the SAC, which releases both acetylcholine and GABA to the DSGC (Fig. 5*E*). However, we found that pharmacological blockade of nicotinic, muscarinic, or $GABA_A$ receptors in the retina with DHbE, atropine, or gabazine, respectively, did not prevent the sensitization of the pDSGC spiking activity (Fig. 5*F*). This suggested that the sensitization of the pDSGC arises from enhanced glutamate release from bipolar cells.

Glycinergic signaling in the Off pathway contributes to sensitized glutamatergic inputs to dorsal pDSGCs

Previous studies in the vertebrate retina indicate that enhanced bipolar cell glutamate release can result from adapted presynaptic inhibition of bipolar cell terminals (Kastner and Baccus, 2013; Nikolaev et al., 2013; Mazade and Eggers, 2016; Appleby and Manookin, 2019; Kastner et al., 2019). Since blocking $GABA_A$ receptor signaling did not affect pDSGC sensitization (Fig. 5*F*), we next blocked another major type of presynaptic inhibition, glycinergic signaling (Diamond, 2017), by bath application of strychnine while recording from dorsal pDSGCs before and after the induction stimulus. We found that glycinergic blockade significantly reduced the sensitization of dorsal pDSGC spiking activity and PSP during On and Off responses, and between test spots (Fig. 6*A–D*). The Off and sustained component of EPSCs also showed reduced sensitization. However, the sensitization index of the On EPSC was not affected by strychnine despite the impaired sensitization of On spiking responses (Fig. 6*E*, *F*), indicating that the sensitization of On EPSCs is not sufficient to offset sensitized IPSCs (Fig. 6*G*) and to induce sensitization of On spiking responses in dorsal pDSGCs.

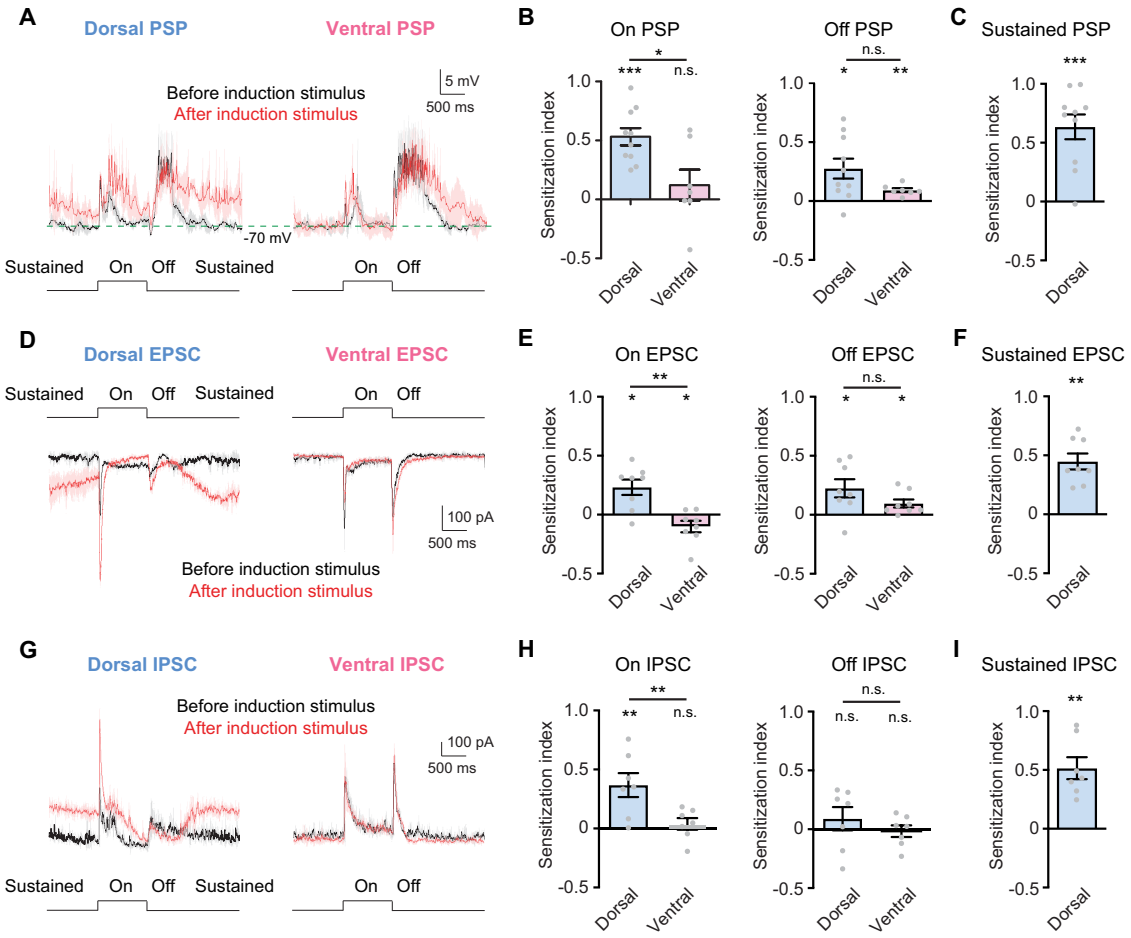

Figure 4. Membrane potential and synaptic currents of dorsal and ventral pDSGCs show distinct sensitization patterns. ***A***, Example PSP traces of dorsal and ventral pDSGCs evoked by test spots before (black) and after (red) induction stimulus. PSP traces represent trial average (darker traces) and SEM (lighter traces). Note that in the dorsal PSP trace, there is a sustained component of elevated depolarization that persists during the time window between the test spot offset and the onset of the next test spot. ***B***, Summary plots comparing the sensitization indices of PSPs between dorsal and ventral pDSGCs. Dorsal, $n = 10$ cells from 4 mice; ventral, $n = 7$ cells from 4 mice. For On PSP: dorsal, $^{***}p < 0.001$; ventral, $p = 0.39$; dorsal versus ventral, $^{*}p = 0.014$. For Off PSP: dorsal, $^{*}p = 0.017$; ventral, $^{**}p = 0.0035$; dorsal versus ventral, $p = 0.11$. ***C***, Summary graph of the sensitization index of the sustained component of PSPs from dorsal pDSGCs. $N = 10$ cells from 4 mice, $^{***}p < 0.001$. ***D***, Example EPSC traces of a dorsal and a ventral pDSGC evoked by test spots before (black) and after (red) induction stimulus. PSC traces represent the trial average (darker traces) and SEM (lighter traces) for this and subsequent figures. Note that in the dorsal pDSGC EPSC, there is a sustained inward current that persists during the time window between the test spot offset and the onset of the next test spot. Such a sustained component was not observed in the ventral pDSGCs. ***E***, Same as ***B***, but for On and Off EPSCs. Dorsal, $n = 8$ cells from 6 mice; ventral, $n = 8$ cells from 5 mice. Dorsal On EPSC peak amplitude value after sensitization is relative to the elevated baseline tonic current. For On EPSC: dorsal, $^{*}p = 0.030$; ventral, $^{*}p = 0.026$; dorsal versus ventral, $^{**}p = 0.0042$. For Off EPSC: dorsal, $^{*}p = 0.039$; ventral, $^{*}p = 0.036$; dorsal versus ventral, $p = 0.15$. ***F***, Same as ***C***, but for the sustained component of dorsal EPSCs. $N = 8$ cells from 6 mice, $^{**}p = 0.0021$. ***G***, Same as ***D***, but for IPSCs. Note that the sustained component was also observed in the IPSC traces from the dorsal pDSGC but was absent from the ventral pDSGC. ***H***, Comparison of IPSC sensitization indices between dorsal and ventral pDSGCs. Dorsal, $n = 7$ cells from 3 mice; ventral, $n = 7$ cells from 2 mice. For On IPSC: dorsal, $^{**}p = 0.0046$; ventral, $p = 0.38$; dorsal versus ventral, $^{**}p = 0.0014$. For Off IPSC: dorsal, $p = 0.47$; ventral, $p = 0.75$; dorsal versus ventral, $p = 0.50$. ***I***, Same as ***C***, but for the sustained component of IPSCs. $N = 7$ cells from 3 mice, $^{**}p = 0.0035$.

Since a well established role of glycinergic inhibition is to mediate crossover inhibition from the On to the Off pathway via glycinergic AII amacrine cells (Demb and Singer, 2012; Graydon et al., 2018), we tested whether On bipolar cell activity is required for the glycinergic signaling underlying pDSGC sensitization in the Off pathway. We bath applied the mGluR6 agonist L-AP-4 to silence rod and On bipolar cells during visual stimulation. As expected, the On spiking response of the dorsal pDSGC was abolished in L-AP-4. However, we still observed sensitized Off responses and sustained components after the induction stimulus (Fig. 7*A–I*). This result shows that (1) On bipolar cell activity is not involved in the sensitization of Off bipolar cell signaling, and (2) in the dorsal retina, the sustained pDSGC activity between test spots arises from the Off pathway.

Based on the above results, our working model for the sensitization in the Off pathway is that the induction stimulus triggers synaptic depression at the glycinergic synapse from amacrine cells to Off bipolar cells, which leads to increased glutamate release from Off bipolar cells to pDSGCs. Glycinergic disinhibition of Off bipolar cells causes sensitized pDSGC Off responses, as well as sustained depolarization of membrane potential between test spots in dorsal pDSGCs (Fig. 6*H*).

Off-to-On crossover excitation within the bistratified pDSGC dendrites contributes to the sensitization of the On spiking response in the dorsal retina

In dorsal pDSGCs, blocking glycinergic signaling in the retina impaired the sensitization of the On spiking response (Fig. 6*A*, *B*), although the On EPSC was not affected (Fig. 6*E*,*F*), suggesting an alternative glycinergic mechanism underlying the sensitization of the On spiking activity in the dorsal retina. Since the sensitization of dorsal On spiking responses is associated with

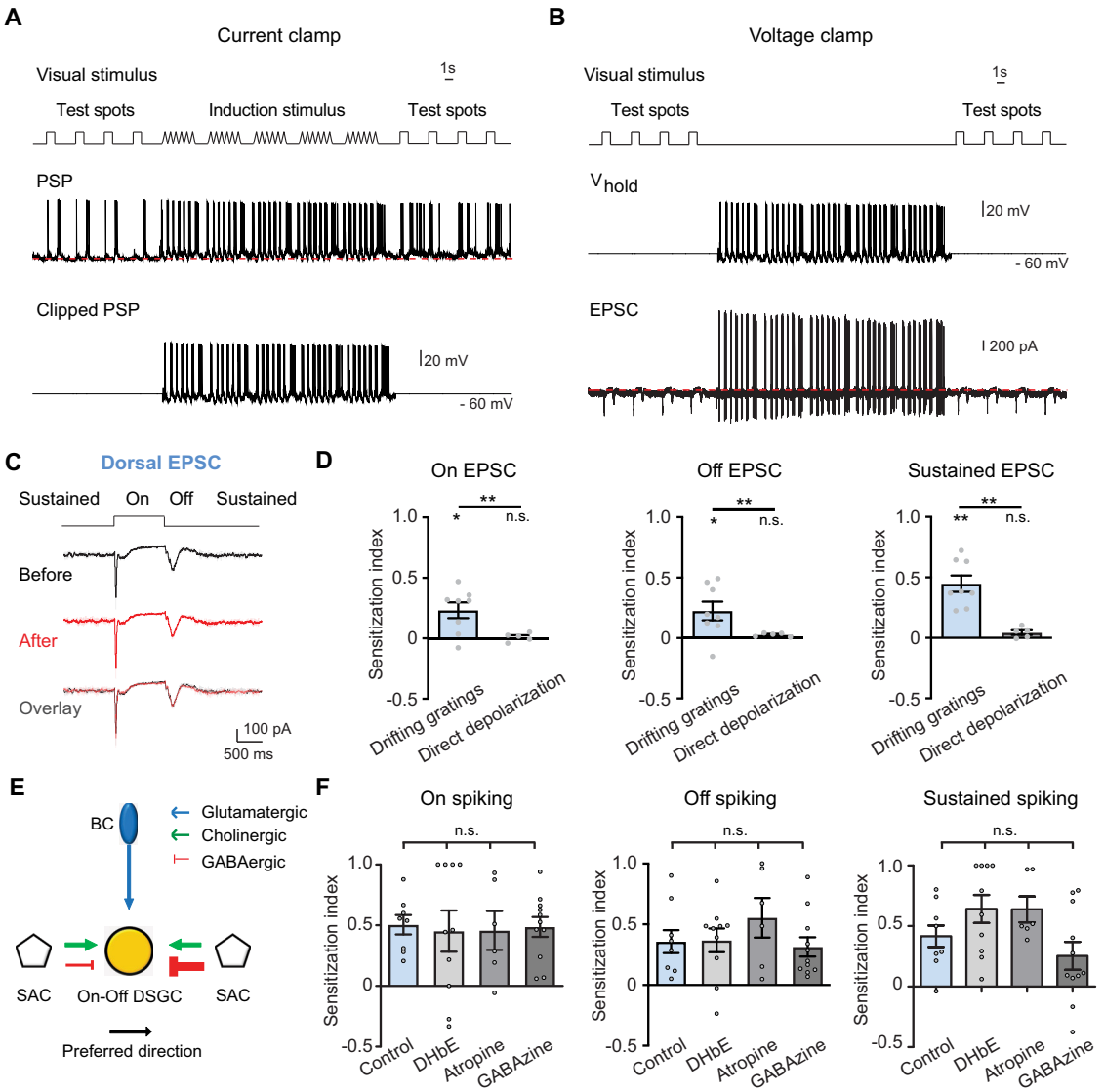

Figure 5. Synaptic inputs to pDSGCs are necessary for the induction of sensitization. ***A***, Top, Schematic shows the complete induction protocol including test spots before and after drifting gratings as the induction stimulus. Middle, Whole-cell current-clamp recording of a pDSGC from the dorsal retina during the visual stimulus shown on the top. Bottom, PSP waveform evoked by drifting gratings was clipped from the PSP trace shown above. ***B***, Top, Schematic shows the visual stimulus protocol with only test spots but without induction stimulus (drifting gratings). Middle, Waveform of the holding potential during whole-cell voltage-clamp recordings of pDSGCs. Bottom, An example EPSC trace from a dorsal pDSGC recorded with the visual stimulus protocol and the holding potential shown above. ***C***, Example EPSC traces of a dorsal pDSGC during test spot stimulus before (black) and after (red) direct depolarization of the pDSGC as a replacement of drifting gratings visual stimulation. This is the same EPSC recording as the one shown in ***B***. Traces are averaged from four repetitions. ***D***, Comparison of the EPSC sensitization indices after drifting grating stimulus ($n = 8$ cells from 6 mice) versus after direct depolarization (no induction visual stimulation; $n = 5$ cells from 2 mice). For On EPSC: drifting gratings, $^{*}p = 0.039$; direct depolarization, $p = 0.60$; drifting gratings versus direct depolarization, $^{**}p = 0.0056$. For Off EPSC: drifting gratings, $^{*}p = 0.040$; direct depolarization, $p = 0.29$; drifting gratings versus direct depolarization, $^{**}p = 0.0018$. For sustained EPSC: drifting gratings, $^{**}p = 0.0014$; direct depolarization, $p = 0.11$; drifting gratings versus direct depolarization, $^{**}p = 0.0024$. ***E***, Simplified schematic shows major types of synaptic inputs onto On-Off DSGCs. BC, Bipolar cell. ***F***, Comparison of the sensitization indices for pDSGC spiking in control (Ames' solution, $n = 8$ cells from 3 mice) or in the presence of different receptor antagonists (DhbE, $n = 10$ cells from 4 mice; atropine, $n = 6$ cells from 2 mice; GABAzine, $n = 11$ cells from 3 mice). One-way ANOVA: for On spiking, $p = 0.99$; for Off spiking, $p = 0.73$; for sustained spiking, $p = 0.14$.

the presence of the sensitized sustained components, both of which are dependent on glycinergic signaling, we hypothesized that this sustained component between test spot trials tonically increases the excitability of dorsal pDSGCs to boost their On spiking responses. We reasoned that if the sustained depolarization of the pDSGC is important for the sensitization of its On spiking response, we would expect to see a positive correlation between the two. We calculated the correlation coefficient between the change of sustained firing rate and that of the On firing rate, and indeed found the sensitization of On spikes strongly correlates to the sensitization of the sustained component (Fig. 7*C*; $^{*}p = 0.047$, coefficient = 0.71), but does not correlate to the sensitization of the Off spikes ($p = 0.15$).

We then measured PSPs and EPSCs of the sustained component after abolishing the On response in the presence of L-AP-4 to study how the signal originating from the Off pathway impacts pDSGC membrane potential during the On stimulus period. In the control group, On EPSC peaks at 58 ± 2 ms after test spot onset, with an average maximal rising slope at 31 ± 7 ms. We found that the sensitized sustained component after the induction stimulus can provide an elevated V_m baseline extending to the first 60 ms after test spot onset (Fig. 7*D–I*), coinciding the On spot-evoked EPSC. Overall, these experimental results

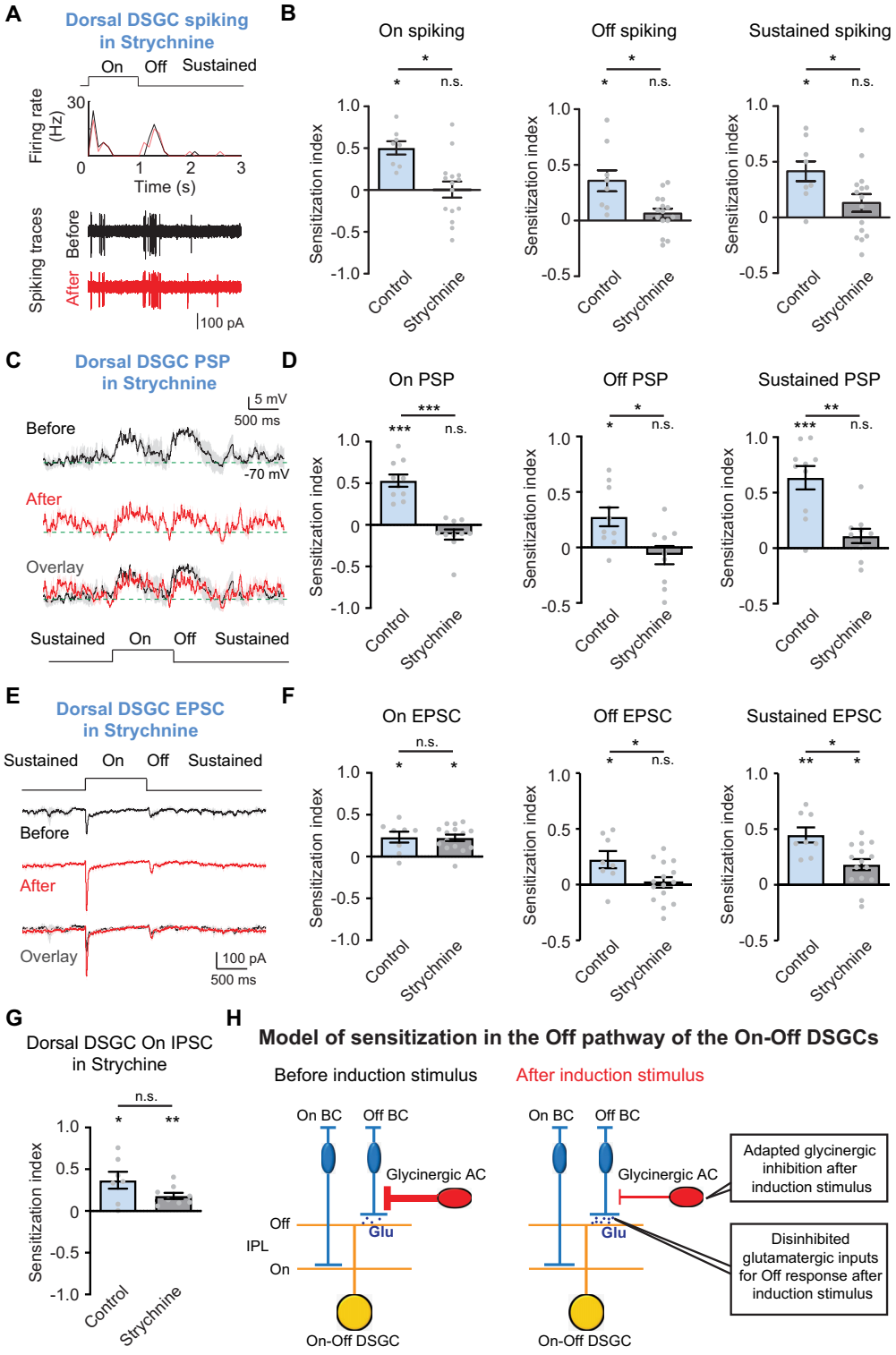

Figure 6. Glycinergic signaling contributes to pDSGC sensitization. ***A***, Example firing rate plot and spiking traces of a dorsal pDSGC responding to test spot stimuli before and after induction stimulus in the presence of strychnine. ***B***, Summary plots comparing the sensitization indices of spiking activity in control (Ames' solution, $n = 8$ cells from 3 mice) and in the presence of strychnine ($n = 15$ cells from 5 mice). For On spiking: control, $^{*}p = 0.016$; strychnine, $p = 0.95$; control versus strychnine, $^{*}p = 0.022$. For Off spiking: control, $^{*}p = 0.012$; strychnine, $p = 0.18$; control versus strychnine, $^{*}p = 0.018$. For sustained spiking: control, $^{*}p = 0.014$; strychnine, $p = 0.16$; control versus strychnine, $^{*}p = 0.047$. ***C***, Example PSP traces of a dorsal pDSGC during test spot stimulus before (black) and after (red) induction stimulus in the presence of strychnine. ***D***, Summary plots comparing the sensitization indices of PSPs in control ($n = 10$ cells from 4 mice) versus in the presence of strychnine ($n = 10$ cells from 3 mice). For On PSP: control, $^{***}p < 0.001$; strychnine, $p = 0.12$; control versus strychnine, $^{***}p < 0.001$. For Off PSP: control, $^{*}p = 0.015$; strychnine, $p = 0.43$; control versus strychnine, $^{*}p = 0.017$. For sustained PSP: control, $^{***}p < 0.001$; strychnine, $p = 0.14$; control versus strychnine, $^{**}p = 0.0011$. ***E***, Example EPSC traces during test spot stimulus before (black) and after (red) induction stimulus in the presence of strychnine. ***F***, Comparison of the EPSC sensitization indices in control ($n = 8$ cells from 6 mice) versus in the presence of strychnine ($n = 15$ cells from 8 mice). For On EPSC: control, $^{*}p = 0.033$; strychnine, $^{*}p = 0.011$; control versus strychnine, $p = 0.93$. For Off EPSC: control, $^{*}p = 0.040$; strychnine, $p = 0.76$; control versus strychnine, $^{*}p = 0.037$. For sustained EPSC: control, $^{**}p = 0.0027$; strychnine, $^{*}p = 0.011$; control versus strychnine, $^{*}p = 0.010$. ***G***, Comparison of the On IPSC sensitization indices in control ($n = 7$ cells from 3 mice) versus in the presence of strychnine ($n = 9$ cells from 6 mice). Control, $^{*}p = 0.016$; strychnine, $^{**}p = 0.0036$; control versus strychnine,

support an important role of the sustained depolarization of the dorsal pDSGC after the induction stimulus in the sensitization of its On response.

How did the sustained depolarization originating from Off bipolar cells influence the On response of the pDSGC? One route is the electrotonic spread of the depolarization in the pDSGC Off dendritic arbor through the soma to the On dendritic arbor (Fig. 8*A*, left). Interestingly, we noted an alternative route for the Off–On cross talk within the bistratified pDSGC dendritic morphology (Fig. 8*A*, right). By two-photon imaging of dye-filled pDSGCs, we noted frequent crossovers of dendritic branches from one dendritic layer to the other. On average, ~30% of the total dendritic arbors of a pDSGC originate from the other layer through crossover dendrites (Fig. 8*B*; 29.5 ± 3.2% of the total dendritic length, mean ± SEM; $n = 21$ cells). The majority of the crossover segments branched from the On layer into the Off layer (Fig. 8*B*,*C*, red dendrites). The majority of the crossover dendrites started diving from one layer to the other at a radial distance of ~40–80 μm away from the soma (Fig. 8*D*,*E*), which mainly falls in the distal half of the pDSGC dendritic field radius (105.3 ± 2.0 μm, $n = 21$ cells).

To assess the functional significance of dendritic crossovers in the signal propagation between On and Off pathways, we constructed a detailed biophysical model of the pDSGC based on the reconstruction of a representative dye-filled cell (Fig. 8*F*, movies). To model the passive electrotonic spread between the dendritic layers, we first simulated a single synaptic input from a bipolar cell with a current injection (70 pA; duration, 100 ms; Fig. 8*F*, Movies 1, 2, 3, 4, 5). This input was placed at different locations throughout the Off dendritic arbor of the pDSGC, while the membrane potential changes in both the On and Off dendritic layers were monitored (Movies 6, 7, 8, 9, 10). In this simulation, only passive membrane properties of the pDSGC were included. We found that dendritic crossovers provide shortcuts for fast and efficient electrotonic spread of depolarization from the Off layer to the On layer bypassing the soma (Fig. 8*F*, Movies 1, 2, 3, 4, 5, 6, 7, 8, 9, 10). Therefore, the direct route through dendritic crossovers provides plausible physical substrates for the cross-layer influence of sustained Off bipolar cell inputs on the On responses of dorsal pDSGCs during sensitization.

Next, we examined the role of active dendritic mechanisms in sensitizing the On spiking response in dorsal pDSGCs. Previous studies indicate that On-Off DSGC dendrites are equipped with nonlinear integration mechanisms including NMDA receptors and dendritic spike initiation, which contribute to the dendritic processing of motion signals (Oesch et al., 2005; Schachter et al., 2010; Stafford et al., 2014; Poleg-Polsky and Diamond, 2016). Therefore, we included these conductances in two active pDSGC models, one containing NMDA receptors and a somatic spiking mechanism that included Na^+ and K^+ channels (Movies 11, 12, 13), and the other containing both NMDA receptors and a dendritic spiking mechanism (Movies 14, 15, 16). To mimic what we observed in experimental recordings, an Off spot presented to one side of the dendritic field (diameter, 100 μm; duration, 50 ms) evoked local Off bipolar cell inputs to the Off dendrites with a sustained component. The On response was evoked with a local On spot stimulus (diameter, 100 μm; duration, 10 ms; delayed from the Off spot by 20 ms) presented to the same location (Movies 11, 14) or a different location (Movies 12-13, 15-16). A passive model (Movies 17, 18, 19) was stimulated with the same Off and On spots, but had no NMDA receptors or voltage-gated channels. Compared with the passive pDSGC model (Movies 17-19), active models (Movies 11, 12, 13, 14, 15, 16) showed a pronounced effect in supralinear summation and sensitization of the On spiking subsequent to the sustained component. The models also suggested that the supralinear summation via crossover dendrites occurs locally between vertically aligned On and Off dendritic regions (Movie 11 vs Movies 12, 13; Movie 14 vs Movies 15, 16), because the sustained depolarization from local Off bipolar cell inputs is more effective in recruiting nonlinear voltage-dependent mechanisms and triggering suprathreshold events at a shorter electrotonic distance. Consistent with the modeling result, we found experimentally that the local induction of sensitization more effectively enhanced the local On response at the same site than that at the opposite site (Fig. 8*G*).

Based on the above experimental and modeling results, our working model for the sensitized pDSGC On response in the dorsal retina is that after the induction stimulus, dorsal pDSGCs receive enhanced tonic glutamatergic inputs from Off bipolar cells, which depolarize the membrane potential and propagate to the On dendritic layers of pDSGCs, increasing the dendritic excitability of the cell. As a result, the subsequent On stimulus triggers a stronger On response (Fig. 7*J*, dorsal). In contrast, ventral pDSGCs lack the sustained depolarization after the induction stimulus, and therefore did not exhibit sensitized On responses (Fig. 7*J*, ventral).

Development of neural sensitization in pDSGCs

Since the sensitization of the pDSGC depends on the glycinergic circuitry that shapes the Off bipolar cell activity, we postulated that the development of the sensitization should coincide with the period when bipolar cell connectivity matures. Previous studies in rodents have shown that the integration of Off bipolar cells into the retinal network starts at approximately P8 and continues for several weeks after the eye opening at P14 (Olney, 1968; Fisher, 1979; Sassoè-Pognetto and Wässle, 1997; Tian and Copenhagen, 2001; Sherry et al., 2003; He et al., 2011; Stafford et al., 2014). We did not detect sensitization of either On or Off spiking responses of dorsal pDSGCs at the early stage of bipolar cell innervation at P12 to P13; nor did we detect the sustained component in dorsal pDSGCs at this stage (Fig. 9*A*,*C*). Therefore, the emergence of the sensitization and the sustained component of pDSGC occurs after eye opening, which overlaps with the maturation timeline of both glycinergic inhibition and bipolar cell connectivity in the rodent retina (Fisher, 1979; Sassoè-Pognetto and Wässle, 1997).

We next asked whether the visual experience after eye opening is required for the development of pDSGC sensitization. We reared mice in the dark from P8 to P36 and then compared the sensitization indices of pDSGCs from these mice to those of the controls. Dark rearing did not alter the normal pattern of sensitization: dorsal cells still exhibited sustained elevation of baseline firing and enhanced light responses to test spots after the induction stimulus (Fig. 9*B*,*C*). Therefore, the sensitization of pDSGCs developed after eye opening but was independent of visual experience.

←

$p = 0.076$. ***H***, A mechanistic model of sensitization in the Off pathway of the direction-selective circuit. Schematic diagrams show side views of the laminar organization of bipolar cells (BCs), glycinergic amacrine cells (ACs), and On-Off DSGCs in the IPL. In the Off pathway, the presynaptic glycinergic AC adapts and disinhibits Off BC after induction stimulus. Therefore, the DSGC Off responses are enhanced because of higher glutamate release from Off BCs.

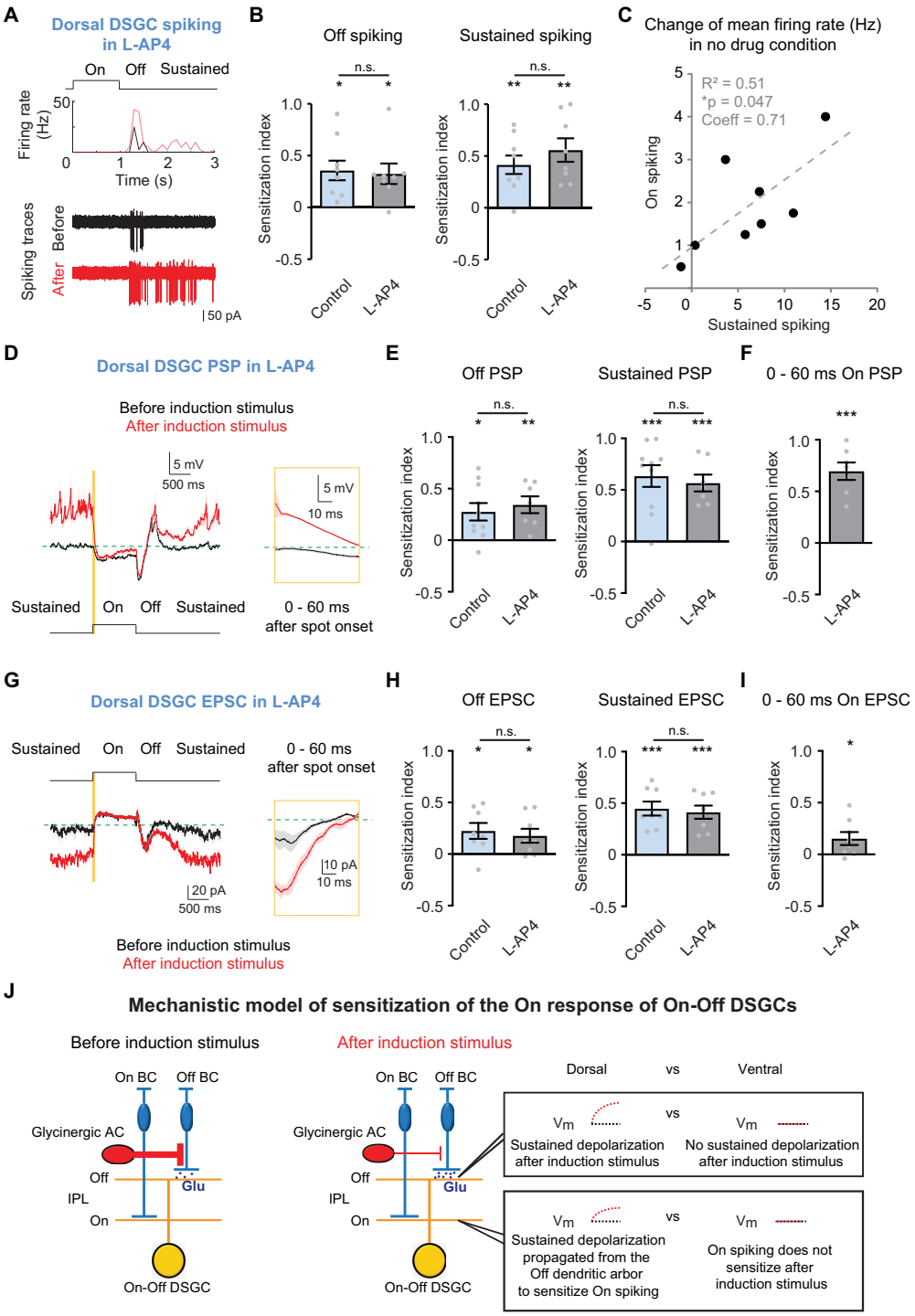

Figure 7. Sensitization of the sustained component from the Off pathway contributes to On sensitization. ***A***, Example firing rate plot and spiking traces of a dorsal pDSGC responding to test spot stimuli before and after induction stimulus in the presence of L-AP-4. ***B***, Summary graphs comparing the sensitization indices for the Off and the sustained components of spiking activity in control (Ames' solution, $n = 8$ cells from 3 mice) versus in the presence of L-AP-4 ($n = 8$ cells from 3 mice). For Off spiking: control, $^{*}p = 0.011$; strychnine, $^{*}p = 0.020$; control versus strychnine, $p = 0.81$. For sustained spiking: control, $^{**}p = 0.0096$; strychnine, $^{**}p = 0.0054$; control versus strychnine, $p = 0.40$. ***C***, Scatter plot comparing the increase of firing rates of the On spiking response versus that of the sustained component. Black dots represent individual cells ($n = 8$ cells from 3 mice), and the dashed line indicates linear regression fit. ***D***, Example PSP traces of a dorsal pDSGC during test spot stimulus before (black) and after (red) induction stimulus in the presence of L-AP-4. ***E***, ***F***, Summary plots comparing the sensitization indices of PSPs in control ($n = 10$ cells from 4 mice) versus in the presence of L-AP-4 ($n = 7$ cells from 2 mice). For Off PSP: control, $^{*}p = 0.014$; L-AP-4, $^{**}p = 0.0096$; control versus L-AP-4, $p = 0.68$. For sustained PSP: control, $^{***}p < 0.001$; L-AP-4, $^{***}p < 0.001$; control versus L-AP-4, $p = 0.65$ (***E***). For PSP area during 60 ms after test spot onset in the presence of L-AP-4, $^{***}p < 0.001$ (***F***). ***G***, Example EPSC traces during test spot stimulus before (black) and after (red) induction stimulus in the presence of L-AP-4. ***H***, ***I***, Comparison of the EPSC sensitization indices in control ($n = 8$ cells from 6 mice) versus in the presence of L-AP-4 ($n = 8$ cells from 3 mice). For Off EPSC: control, $^{*}p = 0.022$; L-AP-4, $^{*}p = 0.035$; control versus L-AP-4, $p = 0.65$. For sustained EPSC: control, $^{***}p < 0.001$; L-AP-4, $^{***}p < 0.001$; control versus L-AP-4, $p = 0.71$ (***H***). For EPSC charge transfer during 60 ms after test spot onset in the presence of L-AP-4, $^{*}p = 0.044$ (***I***). ***J***, A mechanistic model of sensitization of the On responses of On-Off DSGCs. Dorsal DSGC gained an elevated baseline depolarization originating from disinhibition of Off BCs by glycinergic ACs. Such sustained depolarization propagates to On dendritic arbors and enhances the subsequent On response. In contrast, ventral DSGCs do not have sustained depolarization and thus only show sensitized Off responses but not sensitized On responses after induction stimulus.

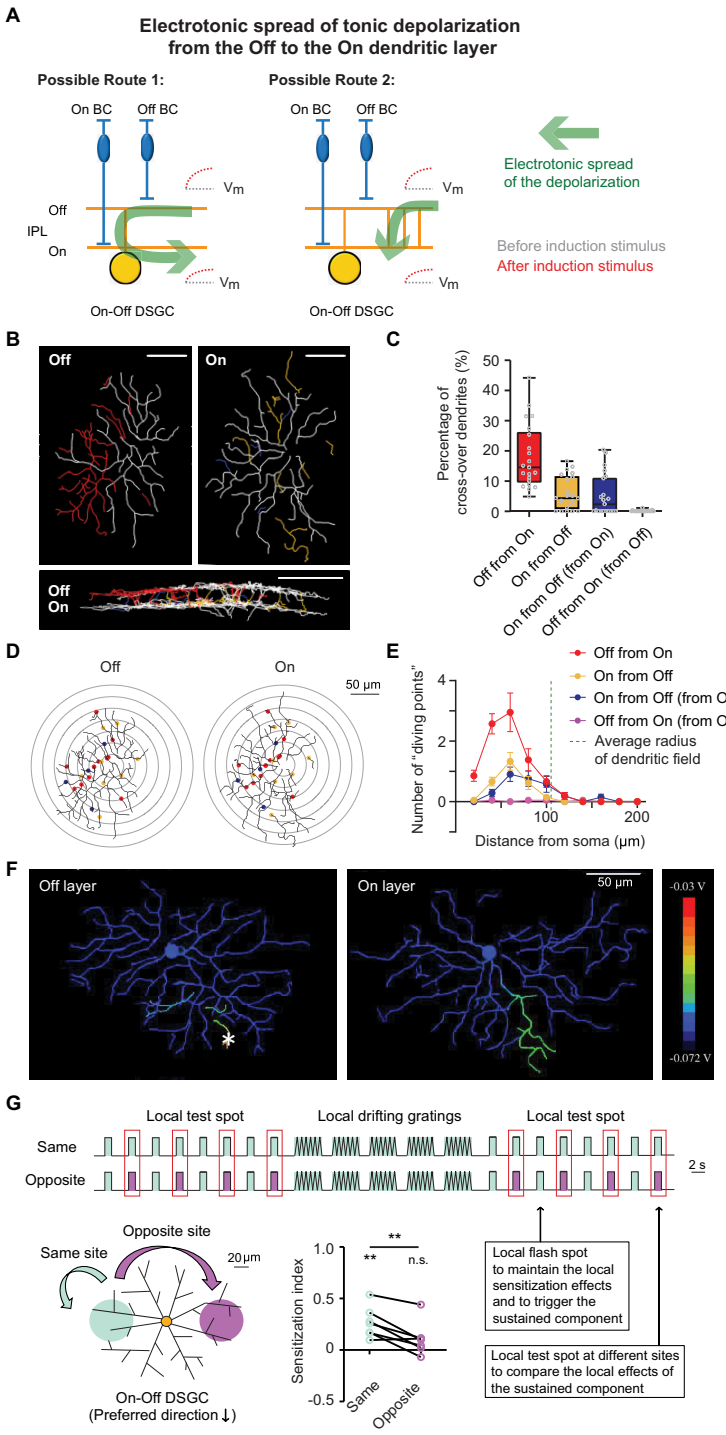

Figure 8. pDSGC dendrites show extensive crossovers between On and Off layers for local interaction between On and Off pathways. ***A***, Schematics showing two possible routes for the electrotonic spread of depolarization from the Off to the On dendritic layers of the bistratified On-Off DSGC. ***B***, Dendritic morphology of an example pDSGC, including dendrites staying in one single layer (white), On dendrites crossing over to the Off layer (red), Off dendrites crossing over to the On layer (yellow), and dendrites from On to Off and then back to On layer (blue). ***C***, Summary box plots representing the percentages of dendritic crossovers over total dendritic lengths. Data were represented as the median ± IQR ($n = 21$ cells). ***D***, The same example cell as in ***B***, but with labels showing the locations of the starting points where dendrites started to cross from one layer to the other ("the diving points"). The colors were coded as ***B*** and ***C***. Concentric rings represent the radial distance from soma. ***E***, Sholl analysis of the diving points ($n = 21$ cells). ***F***, A color map showing a snapshot of the membrane potentials of the pDSGC Off and On layers at 20 ms after a simulated bipolar cell input onto a location (indicated by *) in the Off layer. Model parameters: passive (no voltage-gated channels), Ri = 100 Ω cm, dendritic dia factor = 0.5. For the entire simulation, see Movie 1. ***G***, Sensitization experiment with a local stimulus. Top, Schematics of the stimulus protocols. Bottom left, Diagram of the size and locations of the local stimuli. Bottom right, Comparison of sensitization indices of the spot responses following a sensitized spot response in the local or opposite locations. One-sample *t* test: Local, $^{**}p = 0.0093$; opposite, $p = 0.12$. Paired *t* test: Local versus opposite, $^{**}p = 0.0096$.

Sensitization of other types of RGCs in the mouse retina

The sensitized Off bipolar cell inputs detected in our study may influence multiple postsynaptic targets in addition to pDSGCs. To test whether other RGC types also receive sensitized Off bipolar cell inputs in the dorsal retina, we focused on α-ganglion cells, which can be conveniently targeted by their large soma sizes for recording. On transient (tOn), On sustained (sOn), Off transient (tOff), and Off sustained (sOff) α-cells were identified based on their large soma sizes and typical light responses, as reported previously (Krieger et al., 2017). We noted a subset of RGCs with large somas had sustained Off responses but exhibited biphasic Off spiking activity (Fig. 10*A*; $n = 7$ cells from five mice). Here we tentatively classify them as sOff α-cells. We found that these four types of α-cells had similar levels of peak firing rate (Kruskal–Wallis test, $p = 0.39$), but different baseline firing rates (Kruskal–Wallis test, $^{*}p = 0.040$; Fig. 10*B*), which agrees with previous descriptions (Krieger et al., 2017).

We then calculated the sensitization index of α-cells and found that sOff α-cells also showed sensitization after the induction stimulus (Fig. 10*C*). We noted that the subset of sOff α-cells with biphasic Off responses were located exclusively in the dorsal retina (seven of eight dorsal cells, zero of four ventral cells; Fig. 10*E*). Moreover, only the dorsal biphasic sOff α-cells showed sensitized responses to test spots after the induction stimulus (Fig. 10*D*,*E*). Sensitization of biphasic Off responses in both pDSGCs and sOff α-cells in the dorsal retina supports our working model of sensitized Off bipolar cell sustained signaling in this region.

Discussion

Our finding that the pDSGC responsiveness can be transiently and reversibly sensitized by visual stimulation adds to the accumulating evidence on the contextual modulation of the DSGC response in addition to its robust direction selectivity (Chiao and Masland, 2003; Rivlin-Etzion et al., 2012; Vlasits et al., 2014; Yao et al., 2018; Huang et al., 2019). Notably, dorsal and ventral pDSGCs differ in their sensitization patterns. When sensitization is induced in dorsal pDSGCs, a tonic depolarization originating from Off bipolar cells onto the DSGC Off dendrites readily spreads into the On dendritic layer via crossover dendrites, causes a prolonged

increase of excitability, and boosts the subsequent On spiking responses. In contrast, ventral pDSGCs lack such a sustained elevation of dendritic excitability after induction and therefore are not subject to the relay of sensitization from the Off to the On pathway. Because this dorsal–ventral difference arises from Off bipolar cell modulation, other RGC types that share common Off bipolar cell inputs with pDSGCs may have a similar divergence of sensitization patterns between the dorsal and the ventral retinal regions. Indeed, we found a comparable dorsal–ventral difference in the sensitization pattern of sOff α-cells, which may share common inputs with On-Off DSGCs from type 2 Off cone bipolar cells (Duan et al., 2014; Yu et al., 2018).

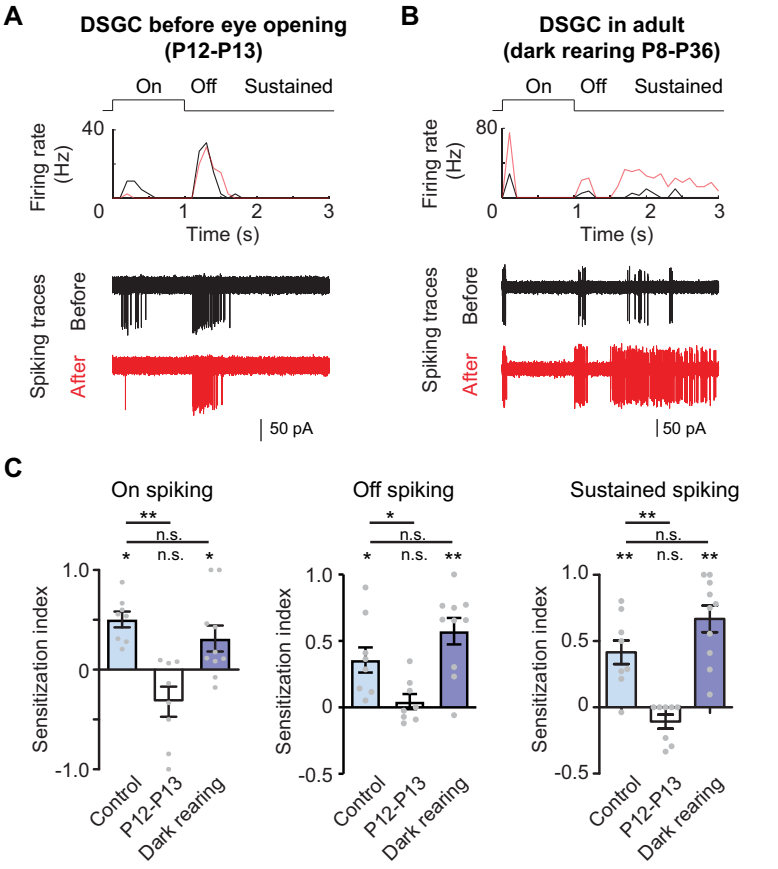

Figure 9. Sensitization of pDSGC light responses develops after eye opening and persists with dark rearing. ***A***, Example firing rate plot and spiking traces of a dorsal pDSGC responding to test spots before and after induction stimulus from a mouse before eye opening at P12. ***B***, Example firing rate plot and spiking traces of a dorsal pDSGC responding to test spots from an adult mouse dark reared during the period P8 to P36. ***C***, Summary graphs comparing the sensitization indices of dorsal pDSGC spiking from control mice ($n = 8$ cells from 3 mice), P12 to P13 mice ($n = 8$ cells from 2 mice), and dark-reared adult mice ($n = 10$ cells from 4 mice). All p values shown here were adjusted with FDR correction. For On spiking: control mice, $^{*}p = 0.013$; P12 to P13 mice, $p = 0.11$; dark-reared mice, $^{*}p = 0.050$; control versus P12 to P13 mice, $^{**}p = 0.0041$; control versus dark-reared mice, $p = 0.54$. For Off spiking: control mice, $^{*}p = 0.012$; P12 to P13 mice, $p = 0.50$; dark-reared mice, $^{**}p = 0.0015$; control versus P12 to P13 mice, $^{*}p = 0.028$; control versus dark-reared mice, $p = 0.16$. For sustained component: control mice, $^{**}p = 0.0048$; P12 to P13 mice, $p = 0.10$; dark-reared mice, $^{**}p = 0.0014$; control versus P12 to P13 mice, $^{**}p = 0.0015$; control versus dark-reared mice, $p = 0.11$.

Topographic differences between dorsal and ventral mouse retina

Different adaptive properties of pDSGC responsiveness in the dorsal and the ventral retinas add to the increasing evidence on the topographic variations in the retinal code. In the mouse retina, dorsal–ventral asymmetry has been reported at multiple stages of visual processing from photoreceptor spectral sensitivity to ganglion cell sizes, densities, and receptive field properties (Wang et al., 2011; Baden et al., 2020; Heukamp et al., 2020; Nadal-Nicolás et al., 2020; Szatko et al., 2020). These specializations on the vertical axis are thought to reflect the adaptation of the retinal circuitry to the different environments in the upper and lower visual fields of the animal. However, in the direction-selective circuit, while extensive studies have focused on the robustness of direction selectivity across the retina under diverse visual conditions, regional differences of the circuit on the vertical axis are underexplored. A decrease in On-Off DSGC dendritic field size from the dorsal to the ventral retina has been reported (El-Danaf and Huberman, 2019). Moreover, On starburst amacrine cells in the dorsal retina can reverse their contrast polarity under certain visual stimulation conditions, a phenomenon that likely originates from region-specific photoreceptor properties and may contribute to the switch of the DSGC directional preference (Rivlin-Etzion et al., 2012; Vlasits et al., 2014; Ankri et al., 2020).

Synaptic mechanisms underlying distinct sensitization patterns of dorsal and ventral pDSGCs

In this study, we found that Off bipolar cell signaling in the dorsal and the ventral retinas is differentially modulated by visual experience, which contributes to the distinct sensitization patterns of postsynaptic RGC targets, including On-Off pDSGCs. An induction stimulus triggers elevated baseline firing and enhanced On and Off responses in dorsal pDSGCs, but only a transient increase of Off responses in ventral cells. Mechanistically, the main difference in sensitization between dorsal and ventral pDSGCs is the presence of a sustained excitatory input in dorsal pDSGCs. pDSGCs receive glutamatergic inputs from bipolar cells and cholinergic inputs from starburst amacrine cells. From a set of pharmacological experiments, we found that the sustained excitatory component is independent of muscarinic acetylcholine receptors (Fig. 5*F*), α-4-containing nicotinic acetylcholine receptors (Fig. 5*F*), or α7 nicotinic acetylcholine receptors (with a-bungarotoxin; data not shown). In addition, the primary rod pathway and the On cone pathway/mGluR6 signaling is not necessary since the sustained component persists in the presence of L-AP-4 (Fig. 7). We have also ruled out a different M/S-opsin ratio (Fig. 3) and GABAA signaling (Fig. 5*F*). Blockage of glycinergic signaling by strychnine significantly reduced the degree of sensitization in the sustained component, (Fig. 6*B*, "sustained spiking", Fig. 6*D*, "sustained PSP") but the sustained excitatory inputs were not completely gone in strychnine (Fig. 6*F*, "sustained EPSC"). The residual sustained excitatory input might be because of intrinsic properties of dorsal Off bipolar cells or because of dorsal-specific circuit or modulatory mechanisms. Future connectomic and physiological comparisons of bipolar cell wiring and response properties between dorsal and ventral retinas may provide new insights into this question.

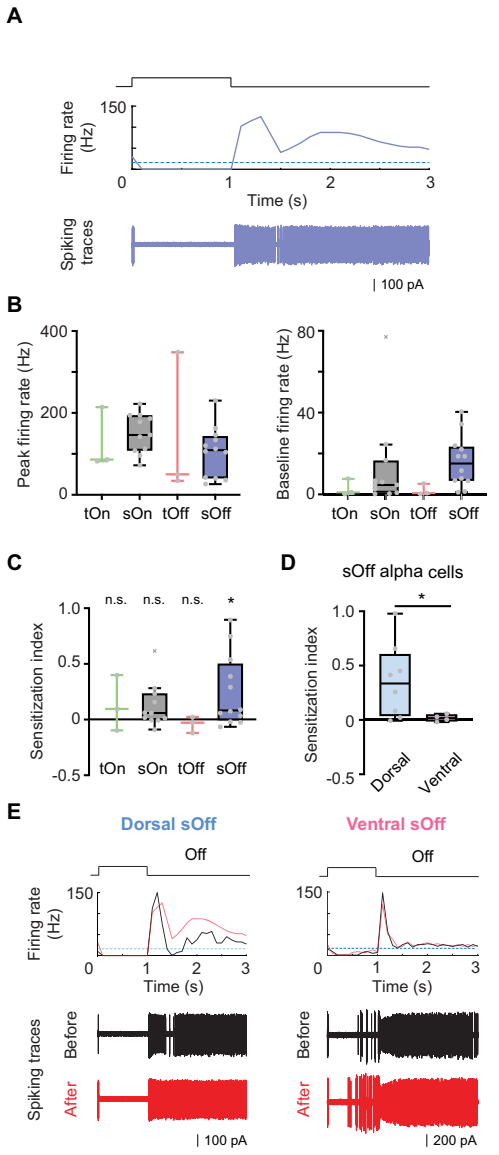

Figure 10. Sensitization is detected in sustained Off α-ganglion cells. ***A***, Firing rate plot and spiking traces of an example cell with biphasic sustained Off response. The horizontal blue dashed line in the firing rate plot indicates baseline firing rate when there was no visual stimulus, and the spiking traces includes four trials of spot responses. ***B***, Peak firing rates and baseline firing rates of four types of α-cells. Sample sizes were represented in the plot. ***C***, Summary box plot of sensitization indices for four types of α-ganglion cells. Single-sample Kolmogorov–Smirnov test: tOn: $n = 3$ cells from 3 mice, $p = 0.75$; sOn: $n = 11$ cells from 9 mice, $p = 0.084$; tOff: $n = 3$ cells from 3 mice, $p = 0.66$; sOff: $n = 12$ cells from 8 mice, $^*p = 0.037$. ***D***, Comparison of the sensitization indices between dorsal ($n = 8$ cells from 5 mice) and ventral ($n = 4$ cells from 3 mice) sOff α-cells. Two-sample Kolmogorov–Smirnov test, $^*p = 0.048$. ***E***, Example firing rate plots and spiking traces of sOff α-cells from the dorsal and the ventral retina during 1-s-duration test spot stimuli before (black) and after (red) induction stimulus.

There are interesting parallels and differences between the sensitization phenomenon observed in our study and the reversal of directional tuning reported in the study by Rivlin-Etzion et al. (2012). Both forms of plasticity can be induced by a short period of strong visual stimulation, and the induction protocol can take multiple forms, including drifting gratings of various directions and spatiotemporal frequencies, and stationary contrast-reversing gratings. Compared with the induction protocols for direction reversal in the study by Rivlin-Etzion et al. (2012), our test spot and induction stimuli are shorter in duration and weaker in intensity. The reversal of direction selectivity observed in the study by Rivlin-Etzion et al. (2012) occurs in a subset of pDSGCs and is long lasting. In contrast, all pDSGCs in this study were desensitized within 20 s in the absence of any visual stimulation and can be repeatedly resensitized (Figs. 1*D*, 2). Mechanistically, both forms of plasticity involve crossover signaling between On and Off pathways. However, distinct synaptic loci appear to underlie the two phenomena. During the reversal of the pDSGC preferred direction, the polarity of SACs switches between On and Off as a result of rod–cone interactions in the outer retina, causing a phase shift between pDSGC excitation and inhibition (Vlasits et al., 2014). This phenomenon is independent of GABAergic and glycinergic signaling. In contrast, the pDSGC sensitization involves a transient glycinergic disinhibition of Off bipolar cells in the inner retina but does not rely on the polarity switch mechanism originating from the outer retinal circuitry. Together, these two forms of plasticity highlight the complexity of contextual modulation during retinal motion processing.

Visual stimuli that induce RGC sensitization

Previous studies on RGC sensitization primarily focused on contrast adaptation, a condition under which induction stimuli have a higher contrast than the test stimulus (Kastner and Baccus, 2011, 2013; Nikolaev et al., 2013; Appleby and Manookin, 2019; Kastner et al., 2019). In this study, we found that the sensitization of pDSGCs can be induced by other forms of visual stimulation, such as moving spots, or drifting and contrast-reversing gratings, at the same contrast as the testing stimulus. Despite different forms of induction stimuli, our results and other studies (Kastner and Baccus, 2011, 2013; Nikolaev et al., 2013; Appleby and Manookin, 2019; Kastner et al., 2019) indicate that RGC sensitization in several species involves short-term disinhibition of bipolar cells. This common mechanistic origin implies that the phenomenon of sensitization is not bound by the category of the induction stimulus per se but reflects the synaptic plasticity rules that permit short-term modulation of bipolar cell signaling under multiple stimulus conditions.

A functional role of crossover dendrites between On and Off dendritic layers of On-Off DSGCs

In the dorsal retina, the tonic elevation of Off bipolar cell inputs after sensitization permits a specific mode of crossover signaling from the Off to the On dendritic layers of the bistratified pDSGC. The electrotonic spread of sustained depolarization from the Off to the On dendritic layers depends on the dendritic architecture and membrane properties. In this context, the dendritic crossovers between the On and the Off layers of On-Off DSGCs, which are evident in published retinal studies (Rivlin-Etzion et al., 2011; Wei et al., 2011) but have not been investigated, are particularly relevant and caught our attention. Here, we provide the first morphologic quantification of this dendritic feature in mouse pDSGCs. We found that dendritic crossover is present in every pDSGC. For a given cell, a significant fraction of dendrites in one layer originates from the other layer. These direct connections between the On and the Off dendritic layers bypassing the soma indicate a more direct route for membrane depolarization to spread between dendritic layers and to recruit voltage-dependent active dendritic mechanisms such as NMDA receptor activation and voltage-gated sodium and calcium channels. Therefore, elevated membrane excitability in the Off dendritic layer can be more readily relayed to the On dendritic layer to sensitize its On spiking

response. Interestingly, studies in the rabbit retina have demonstrated that spikes of On-Off DSGCs are initiated in the dendritic arbors (Oesch et al., 2005; Schachter et al., 2010). In this context, dendritic crossovers may significantly influence local spike initiation in the On layer on sensitization. Both our modeling and experimental results support a role of active dendritic mechanisms in the sensitized spiking activity of dorsal pDSGCs. Future experimental and modeling studies will provide more insights into the functional implications of On-Off DSGC dendritic crossovers during visual processing.

References

Akyuz S, Pavan A, Kaya U, Kafaligonul H (2020) Short- and long-term forms of neural adaptation: an ERP investigation of dynamic motion aftereffects. Cortex 125:122–134.

Ankri L, Ezra-Tsur E, Maimon SR, Kaushansky N, Rivlin-Etzion M (2020) Antagonistic center-surround mechanisms for direction selectivity in the retina. Cell Rep 31:107608.

Applebury ML, Antoch MP, Baxter LC, Chun LL, Falk JD, Farhangfar F, Kage K, Krzystolik MG, Lyass LA, Robbins JT (2000) The murine cone photoreceptor: a single cone type expresses both S and M opsins with retinal spatial patterning. Neuron 27:513–523.

Appleby TR, Manookin MB (2019) Neural sensitization improves encoding fidelity in the primate retina. Nat Commun 10:4017.

Baccus SA, Meister M (2002) Fast and slow contrast adaptation in retinal circuitry. Neuron 36:909–919.

Baden T, Schubert T, Chang L, Wei T, Zaichuk M, Wissinger B, Euler T (2013) A tale of two retinal domains: near-optimal sampling of achromatic contrasts in natural scenes through asymmetric photoreceptor distribution. Neuron 80:1206–1217.

Baden T, Euler T, Berens P (2020) Understanding the retinal basis of vision across species. Nat Rev Neurosci 21:5–20.

Barchini J, Shi X, Chen H, Cang J (2018) Bidirectional encoding of motion contrast in the mouse superior colliculus. Elife 7:e35261.

Barlow HB, Levick WR (1965) The mechanism of directionally selective units in rabbit's retina. J Physiol 178:477–504.

Brainard DH (1997) The Psychophysics Toolbox. Spat Vis 10:433–436.

Chiao C-C, Masland RH (2003) Contextual tuning of direction-selective retinal ganglion cells. Nat Neurosci 6:1251–1252.

Clifford CWG, Wenderoth P, Spehar B (2000) A functional angle on some after-effects in cortical vision. Proc Biol Sci 267:1705–1710.

Cruz-Martín A, El-Danaf RN, Osakada F, Sriram B, Dhande OS, Nguyen PL, Callaway EM, Ghosh A, Huberman AD (2014) A dedicated circuit links direction-selective retinal ganglion cells to the primary visual cortex. Nature 507:358–361.

Demb JB (2008) Functional circuitry of visual adaptation in the retina. J Physiol 586:4377–4384.

Demb JB, Singer JH (2012) Intrinsic properties and functional circuitry of the AII amacrine cell. Vis Neurosci 29:51–60.

Diamond JS (2017) Inhibitory interneurons in the retina: types, circuitry, and function. Annu Rev Vis Sci 3:1–24.

Duan X, Krishnaswamy A, De la Huerta I, Sanes JR (2014) Type II cadherins guide assembly of a direction-selective retinal circuit. Cell 158:793–807.

El-Danaf RN, Huberman AD (2019) Sub-topographic maps for regionally enhanced analysis of visual space in the mouse retina. J Comp Neurol 527:259–269.

Fisher LJ (1979) Development of synaptic arrays in the inner plexiform layer of neonatal mouse retina. J Comp Neurol 187:359–372.

Graydon CW, Lieberman EE, Rho N, Briggman KL, Singer JH, Diamond JS (2018) Synaptic transfer between rod and cone pathways mediated by AII amacrine cells in the mouse retina. Curr Biol 28:2739–2751.e3.

Haverkamp S, Wässle H, Duebel J, Kuner T, Augustine GJ, Feng G, Euler T (2005) The primordial, blue-cone color system of the mouse retina. J Neurosci 25:5438–5445.

He Q, Wang P, Tian N (2011) Light-evoked synaptic activity of retinal ganglion and amacrine cells is regulated in developing mouse retina. Eur J Neurosci 33:36–48.

Heukamp AS, Warwick RA, Rivlin-Etzion M (2020) Topographic variations in retinal encoding of visual space. Annu Rev Vis Sci 6:237–259.

Huang X, Rangel M, Briggman KL, Wei W (2019) Neural mechanisms of contextual modulation in the retinal direction selective circuit. Nat Commun 10:2431.

Huberman AD, Wei W, Elstrott J, Stafford BK, Feller MB, Barres BA (2009) Genetic identification of an on-off direction-selective retinal ganglion cell subtype reveals a layer-specific subcortical map of posterior motion. Neuron 62:327–334.

Jafari M, Ansari-Pour N (2019) Why, when and how to adjust your p values? Cell J 20:604–607.

Kamkar S, Moghaddam HA, Lashgari R (2018) Early visual processing of feature saliency tasks: a review of psychophysical experiments. Front Syst Neurosci 12:54.

Kastner DB, Baccus SA (2011) Coordinated dynamic encoding in the retina using opposing forms of plasticity. Nat Neurosci 14:1317–1322.

Kastner DB, Baccus SA (2013) Spatial segregation of adaptation and predictive sensitization in retinal ganglion cells. Neuron 79:541–554.

Kastner DB, Ozuysal Y, Panagiotakos G, Baccus SA (2019) Adaptation of inhibition mediates retinal sensitization. Curr Biol 29:2640–2651.e4.

Kay JN, De la Huerta I, Kim I-J, Zhang Y, Yamagata M, Chu MW, Meister M, Sanes JR (2011) Retinal ganglion cells with distinct directional preferences differ in molecular identity, structure, and central projections. J Neurosci 31:7753–7762.

Khani MH, Gollisch T (2017) Diversity in spatial scope of contrast adaptation among mouse retinal ganglion cells. J Neurophysiol 118:3024–3043.

Kim JS, Greene MJ, Zlateski A, Lee K, Richardson M, Turaga SC, Purcaro M, Balkam M, Robinson A, Behabadi BF, Campos M, Denk W, Seung HS (2014) Space–time wiring specificity supports direction selectivity in the retina. Nature 509:331–336.

Kim KJ, Rieke F (2001) Temporal contrast adaptation in the input and output signals of salamander retinal ganglion cells. J Neurosci 21:287–299.

Kohn A (2007) Visual adaptation: physiology, mechanisms, and functional benefits. J Neurophysiol 97:3155–3164.

Krieger B, Qiao M, Rousso DL, Sanes JR, Meister M (2017) Four alpha ganglion cell types in mouse retina: function, structure, and molecular signatures. PLoS One 12:e0180091.

Liang L, Fratzl A, Goldey G, Ramesh RN, Sugden AU, Morgan JL, Chen C, Andermann ML (2018) A fine-scale functional logic to convergence from retina to thalamus. Cell 173:1343–1355.e24.

Litvina EY, Chen C (2017) Functional convergence at the retinogeniculate synapse. Neuron 96:330–338.e5.

Matulis CA, Chen J, Gonzalez-Suarez AD, Behnia R, Clark DA (2020) Heterogeneous temporal contrast adaptation in Drosophila direction-selective circuits. Curr Biol 30:222–236.e6.

Mazade RE, Eggers ED (2016) Light adaptation alters inner retinal inhibition to shape OFF retinal pathway signaling. J Neurophysiol 115:2761–2778.

Nadal-Nicolás FM, Kunze VP, Ball JM, Peng BT, Krishnan A, Zhou G, Dong L, Li W (2020) True S-cones are concentrated in the ventral mouse retina and wired for color detection in the upper visual field. eLife 9:e56840.

Nikolaev A, Leung K-M, Odermatt B, Lagnado L (2013) Synaptic mechanisms of adaptation and sensitization in the retina. Nat Neurosci 16:934–941.

Oesch N, Euler T, Taylor WR (2005) Direction-selective dendritic action potentials in rabbit retina. Neuron 47:739–750.

Olney JW (1968) An electron microscopic study of synapse formation, receptor outer segment development, and other aspects of developing mouse retina. Invest Ophthalmol 7:250–268.

Poleg-Polsky A, Diamond JS (2016) NMDA receptors multiplicatively scale visual signals and enhance directional motion discrimination in retinal ganglion cells. Neuron 89:1277–1290.

Rieke F, Rudd ME (2009) The challenges natural images pose for visual adaptation. Neuron 64:605–616.

Rivlin-Etzion M, Zhou K, Wei W, Elstrott J, Nguyen PL, Barres BA, Huberman AD, Feller MB (2011) Transgenic mice reveal unexpected diversity of on-off direction-selective retinal ganglion cell subtypes and brain structures involved in motion processing. J Neurosci 31:8760–8769.

Rivlin-Etzion M, Wei W, Feller MB (2012) Visual stimulation reverses the directional preference of direction-selective retinal ganglion cells. Neuron 76:518–525.

Rosa JM, Morrie RD, Baertsch HC, Feller MB (2016) Contributions of rod and cone pathways to retinal direction selectivity through development. J Neurosci 36:9683–9695.

Sanes JR, Masland RH (2015) The types of retinal ganglion cells: current status and implications for neuronal classification. Annu Rev Neurosci 38:221–246.

Sassoè-Pognetto M, Wässle H (1997) Synaptogenesis in the rat retina: subcellular localization of glycine receptors, GABA(A) receptors, and the anchoring protein gephyrin. J Comp Neurol 381:158–174.

Schachter MJ, Oesch N, Smith RG, Taylor WR (2010) Dendritic spikes amplify the synaptic signal to enhance detection of motion in a simulation of the direction-selective ganglion cell. PLoS Comput Biol 6: e1000899.

Schwartz O, Hsu A, Dayan P (2007) Space and time in visual context. Nat Rev Neurosci 8:522–535.

Sethuramanujam S, Yao X, deRosenroll G, Briggman KL, Field GD, Awatramani GB (2017) "Silent" NMDA synapses enhance motion sensitivity in a mature retinal circuit. Neuron 96:1099–1111.e3.

Sherry DM, Wang MM, Bates J, Frishman LJ (2003) Expression of vesicular glutamate transporter 1 in the mouse retina reveals temporal ordering in development of rod vs. cone and ON vs. OFF circuits. J Comp Neurol 465:480–498.

Shi X, Barchini J, Ledesma HA, Koren D, Jin Y, Liu X, Wei W, Cang J (2017) Retinal origin of direction selectivity in the superior colliculus. Nat Neurosci 20:550–558.

Smith RG (1992) NeuronC: a computational language for investigating functional architecture of neural circuits. J Neurosci Methods 43:83–108.

Stafford BK, Park SJH, Wong KY, Demb JB (2014) Developmental changes in NMDA receptor subunit composition at ON and OFF bipolar cell synapses onto direction-selective retinal ganglion cells. J Neurosci 34:1942–1948.

Szatko KP, Korympidou MM, Ran Y, Berens P, Dalkara D, Schubert T, Euler T, Franke K (2020) Neural circuits in the mouse retina support color vision in the upper visual field. Nat Commun 11:3481.

Theeuwes J (2013) Feature-based attention: it is all bottom-up priming. Philos Trans R Soc Lond B Biol Sci 368:20130055.

Tian N, Copenhagen DR (2001) Visual deprivation alters development of synaptic function in inner retina after eye opening. Neuron 32:439–449.

Vlasits AL, Bos R, Morrie RD, Fortuny C, Flannery JG, Feller MB, Rivlin-Etzion M (2014) Visual stimulation switches the polarity of excitatory input to starburst amacrine cells. Neuron 83:1172–1184.

Wang YV, Weick M, Demb JB (2011) Spectral and temporal sensitivity of cone-mediated responses in mouse retinal ganglion cells. J Neurosci 31:7670–7681.

Wark B, Fairhall A, Rieke F (2009) Timescales of inference in visual adaptation. Neuron 61:750–761.

Warwick RA, Kaushansky N, Sarid N, Golan A, Rivlin-Etzion M (2018) Inhomogeneous encoding of the visual field in the mouse retina. Curr Biol 28:655–665.e3.

Wei W, Hamby AM, Zhou K, Feller MB (2011) Development of asymmetric inhibition underlying direction selectivity in the retina. Nature 469:402–406.

Yao X, Cafaro J, McLaughlin AJ, Postma FR, Paul DL, Awatramani G, Field GD (2018) Gap junctions contribute to differential light adaptation across direction-selective retinal ganglion cells. Neuron 100:216–228.e6.

Yu W-Q, El-Danaf RN, Okawa H, Pacholec JM, Matti U, Schwarz K, Odermatt B, Dunn FA, Lagnado L, Schmitz F, Huberman AD, Wong ROL (2018) Synaptic convergence patterns onto retinal ganglion cells are preserved despite topographic variation in pre- and postsynaptic territories. Cell Rep 25:2017–2026.e3.